Ana Catarina Tavares Pinheiro

Bachelor of Science in Engineering of Micro and Nanotechnology

Luminescent Glass Materials for Photovoltaics

Dissertation to obtain the master's degree in

Engineering of Micro and Nanotechnology

Supervisor: Dr. César Laia, Assistant Professor, NOVA University of Lisbon

Co-supervisor: Dr. Hugo Águas, Associate Professor, NOVA University of Lisbon

Jury

President: Dr. Rodrigo Ferrão de Paiva Martins

Examiner: Dra. Márcia Vilarigues Gomes

Member: Dr. César António Tonicha Laia

FACULDADE DE CIÊNCIAS E TECNOLOGIA
UNIVERSIDADE NOVA DE LISBOA

October, 2019

Luminescent Glass Materials for Photovoltaics

"And spite of all dogmas, current in all ages,
one settled fact is better than ten sages."
— Edgar Allan Poe

Acknowledgments

Primeiramente, gostaria de demonstrar a minha gratidão para com o Professor Rodrigo Martins e a Professora Elvira Fortunato, por serem os fundadores deste extraordinário curso, que tive o prazer de poder chamar de "meu" ao longo destes últimos 5 anos, e que me proporcionou uma nova visão, no que toca à ciência como ferramenta para a inovação e desenvolvimento da sociedade.

Com um carinho especial, quero agradecer ao Professor César Laia e ao Professor Hugo Águas, como meus orientador e co-orientador, respetivamente, por me terem dado a oportunidade de trabalhar com um tema que me suscita extremo interesse e, como meus professores, por terem tido participação direta na minha formação como aluna desta instituição. Aos nomes seguidamente enunciados, um grande obrigada por todo o apoio prestado no decorrer deste projeto de mestrado: Sandra Gago, Andreia Ruivo, Carina Figueiredo, Deneb Menda, Ana Santa, Tiago Mateus, Tiago Moreira, Sara Silvestre, Joana Pinto e Vidreira Infante, LDA. Um agradecimento aos restantes professores que me acompanharam e formaram ao longo do meu percurso académico.

Quero agradecer a todos os meus colegas, que no decorrer destes 5 anos, estiveram presentes, quer nos momentos de desespero pré-entrega de trabalhos, quer nos momentos de folia e de jola na mão. Ao manito Carlos, por todo apoio, risadas e cusquices. À minha *sista* Maria, por me ajudar sempre a saber lidar. À frendona Rita, pela genuinidade e amizade. Ao *homeboy* Teles, por ser extremamente hilariante. Ao Miguéu, por toda ajuda e companhia. Ao Fabiu, pelas risadas. À Débora, ao Chapa e ao Lima, pela *guidance*. Ao meu afilhado *Tommy Boy* pelo *sass* e à minha filhada Inês Damasco pelo amor ao *holo*. À Catarina Marques por todo o apoio e auxílio.

Às minhas companheiras de longa data, Clarisse Silva, Carolina Pacheco e Beatriz Soromenho, obrigada por todos os momentos, que guardarei com carinho, e pelo interesse demonstrado na minha ocupação, como estudante.

Aos meus pais, Joaquim e Paula, quero deixar o maior dos agradecimentos, por me apoiarem incondicionalmente e me proporcionarem, com os frutos do seu esforço e trabalho, muitas das oportunidades da minha vida. Aos meus avós, Nelson e Ermelinda, que tiveram um impacto tremendo na minha vida e ajudaram a moldar a pessoa que hoje

tenho orgulho em ser. A toda a família, um grande obrigada por todo o apoio e orgulho que depositam em mim.

Quero, também, agradecer ao meu namorado e melhor amigo, Gui, pelo apoio e dedicação em mim depositados ao longo destes 6 anos de namoro, para além de toda a paciência e compreensão, as quais são indispensáveis para aturar a minha animada, mas chatinha, pessoa.

Por fim, mas não menos importante, quero agradecer ao Projeto "InLumGlass" (PTDC/QEQ-QIN/3007/2014), apoiado pela Fundação para a Ciência e a Tecnologia e em parceria com a Universidade de Aveiro.

Abstract

The increasingly demand for clean and renewable energy generation accounts for the need for highly efficient energy conversion systems, at a reduced manufacturing cost. In this project, two different approaches to the conventional Luminescent Solar Concentrator (LSC) are conceived, where a LSC consists of an host matrix, which comprises luminescent species that absorb a certain wavelength range of the incident light posteriorly re-emitting this light at a different wavelength. By application of Inorganic Perovskite Quantum Dots (IPQDs) as luminophores in these devices it is possible to modulate their bandgap to correspond to the maximum of efficiency of the Photovoltaic (PV) device that is to be coupled to the LSC.

Cesium-lead-bromide ($CsPbBr_3$) IPQDs were synthetized, by hot-injection method, and deposited over different glass-comprising substrates, via spin-coating, creating a uniform thin film. The first analysed substrates were glass samples in which a group of four microcrystalline silicon PV cells were deposited and posteriorly coated with the IPQDs. The remaining analysed glass substrates were coated with the IPQDs and either coupled on top of an organic PV module or integrated in a 3D structure, which was covered with aluminium and it comprised two glass samples. These glasses were coated with IPQDs and put, side by side, inside the 3D structure in order to create a fully transparent LSC and explore its photovoltaic applications, together with the possibility of integration of this device as, has it is generally categorized, a smart window in building façades. A optical efficiency value of 3.72% was obtained for a LSC system coupled to an organic PV module, in the luminescent geometry.

Keywords: Photovoltaic, Perovskite Quantum Dots, Down-Shifting, Luminescent Solar Concentrator, Smart Windows.

Resumo

A crescente procura de formas de produção de energia limpas e renováveis resulta da necessidade de sistemas de conversão de energia com elevadas eficiências, a um custo de manufatura reduzido. Neste trabalho, foram concebidas duas abordagens diferentes ao Concentrador Solar (LSC) convencional, onde um LSC consiste numa matriz que contém espécies luminescentes que absorvem a luz incidente de um certo comprimento de onda reemitindo-o, posteriormente, a um comprimento de onda diferente. Através da aplicação de Quantum Dots Inorgânicos de Perovskite (IPQDs) é possível modelar o seu hiato energético de forma a este corresponder ao máximo de eficiência do dispositivo Fotovoltaico (PV) a ser acoplado ao LSC.

Foram sintetizados QDs de césio, chumbo e bromo ($CsPbBr_3$) através do método de *hot-injection* e depositados em diferentes substratos contendo vidro inorgânico, via *spin-coating*, para a criação de um filme fino uniforme. Os primeiros substratos analisados consistiam em amostras de vidro, onde um grupo de quatro células PVs de silício microcristalino foram depositadas e, posteriormente, cobertas com IPQDs. As restantes amostras de vidro analisadas foram cobertas com IPQDs e seguidamente, ou acopladas no topo de um modulo PV orgânico, ou integradas numa estrutura 3D. Esta estrutura 3D foi coberta internamente com alumínio, onde os substratos de vidro cobertos com IPQDs foram colocados, lado a lado, dentro da estrutura. Assim, foi possível criar um LSC completamente transparente e explorar as suas aplicações fotovoltaicas, em conjunto com a sua possível integração em fachadas de edifícios como, designação geral, uma janela inteligente. Uma eficiência ótica de 3,72% foi obtida para um sistema LSC acoplado a um módulo PV orgânico, numa geometria de luminescência.

Palavras-chave: Fotovoltaico, *Quantum Dots* de Perovskite, *Down-Shifting*, Concentrador Solar, Janelas Inteligentes.

Contents

List of Figures

List of Tables

Symbols

C_G	geometrical Concentration factor
G	geometrical Gain factor
η_{opt}	optical conversion efficiency
P_{out}	output radiative Power
P_{in}	input radiative Power
A_S	surface Area
A_{Edge}	Edge Area
n	refractive index
2θ	angle between transmitted x-ray beam and reflected beam in degrees

Acronyms

EPBD	Energy Performance of Buildings Directive
EU	European Union
NZEB	Nearly Zero-energy Buildings
PV	Photovoltaic
BIPV	Building Integrated Photovoltaics
TIR	Total Internal Reflection
QD	Quantum Dot
TSC	Transparent Solar Concentrator
PMMA	Poly (Methyl Methacrylate)
PC	Polycarbonate
PL	Photoluminescence
PQD	Perovskite Quantum Dot
QY	Quantum Yield
UV-vis	Ultraviolet-visible
I**PQD**	Inorganic Perovskite Quantum Dot
OA	Oleic Acid
ODE	Octadecene
OAM	Oleylamine
UV	Ultraviolet
CVD	Chemical Vapor Deposition
SEM	Scanning Electron Microscopy
STEM	Scanning Transmission Electron Microscopy
XRD	X-Ray Diffraction
TLSC	Transparent and Luminescent Solar Concentrator
EQE	External Quantum Efficiency
NPL	Nanoplate

FWHM Full Width Height Maximum

IZO Indium-Zinc Oxide

PCE Power Conversion Efficiency

Motivation and objectives

Due to an increase of fossil fuels and other non-renewable energy sources exploration, mainly triggered by the rapid industry expansion and worldwide technological evolution, actions must be taken in order to assure and improve quality of life for the future generations, without jeopardizing the environmental health of our planet and socio-economic stability. To mitigate this negative impact, recent technological trends show us an increased interest in the development of high-performance smart devices for energy harvesting, conversion and storage.

Recently, the European Commission legislated a series of recommendations on the modernisation of buildings known has the Energy Performance of Buildings Directive (EPBD), since the building sector is the number one largest energy consumer in the EU. From these recommendations, it is shown that the EU is strongly committed towards achieving a fully sustainable and decarbonised system by 2050, with the extent that all buildings must be Nearly Zero-Energy Buildings (NZEB) by 2020. [1]–[3]

This gives rise to a new market in the actual building industry, more specifically when it comes to the building envelope. A major component of the building envelope is the windows, which can typically range from large to medium areas and its reinvention may lead to a significant impact on energy savings, without compromising its overall performance as a regular window, as well as its affordability. Hence, this project was conducted having the study of Luminescent Solar Concentrators for photovoltaic applications as primary goal, allied to the possibility of its future application in the building industry for energy saving purposes.

1 Introduction

1.1 Luminescent solar concentrators

The fact that nearly 75% of the EUs' buildings remain energy inefficient turns the NZEB directive into a big challenge in terms of implementation. [4] The main obstacles associated with the execution of this directive can be overcome by finding alternatives to conventional solar Photovoltaics (PV) systems.

In highly urbanized and metropolitan areas, the total space required for the installation of enough solar PV modules to meet the electrical demands of this ever-growing population is scarce. Even more, the land costs in such environments makes it economically unreliable to use solar PV systems as a route to reach the NZEB directive. [5] However, the tendency of modern architecture to create a huge disparity between the total ground and rooftop area, when compared to the total building height and envelope area, gave rise to the development of Building Integrated Photovoltaics (BIPV). [6], [7] Not only is it possible to have PV elements becoming an integral component of the building envelope, but also, we may overlook on the downsides inherent to traditional PV systems, such as low power conversion efficiencies and susceptibility to partial shading, dirt, thermal gradients, or aging. [8]

1.1.1. Operation principle

The idea of Luminescent Solar Concentrator (LSC) arose from the need of lowering the cost of solar modules. Their concept is being explored since the 70's and their primary advantages include their independence on the incident irradiance angle, their use of both direct and diffuse sunlight, separate optimization of the light harvesting and the energy conversion cells, high defect tolerance and low-level cost. [9]–[11]

The operating principle of LSCs is based on three main mechanisms: absorption, luminescence and trapping/transportation of light. Accordingly, the portion of the solar spectrum is absorbed by luminescing species, which are embedded in either a plastic host matrix or an inorganic glass substrate functionalized with a surface coating of such species, commonly referred to as glazing. This functionalization can occur by integration of luminophores inside the matrix of the material or via a liquid solution between the vitreous plates. These host materials act as optical waveguides, where the incident light is absorbed and re-emitted. Here, a portion of this light is trapped in the waveguide-like structure and

concentrated, through Total Internal Reflection (TIR), towards the edges of the overall structure. The total radiation that is concentrated on the edges of the LSC can then be focused onto a highly efficient PV solar cell, localized on one or more of these edges, in order to optimize the performance of the PV conversion devices. Part of the operation mechanism of a LSC is displayed in figure 1.1. [10], [12]–[15]

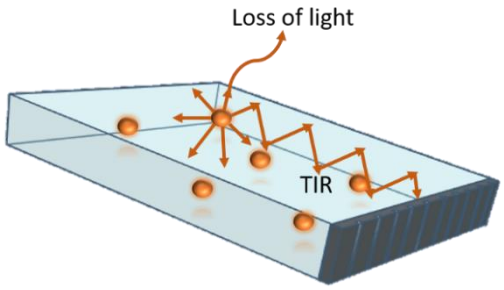

Figure 1.1: Principle of operation of a LSC, in a traditional "luminescence geometry" configuration, post luminophore light absorption and emission.

Re-absorption losses are crucial for the reduction of the overall LSC system efficiency. These occur when the light emitted by the luminescing species is absorbed, once again, by a neighbour luminescent particle, instead of being guided by the waveguide into the solar cell. Hence, the quantum yield of the luminophore, the waveguiding efficiency, the Stokes shift of the luminophore absorption and emission spectrum and the overall dimensions of the waveguide material need to be finely tuned in order to overcome such losses. [11], [16]

1.1.2. Geometry, materials and characterization

In LSCs, geometry plays an essential role on the total power of the radiation that is concentrated by the waveguide structure and directed into the PV device on the edge of such structure.

LSCs are characterized in terms of a geometrical concentration factor (C_G), which is defined as the product of the geometrical gain factor (G) with the optical conversion efficiency (η_{opt}) of the overall waveguide structure.

$$C_G = \eta_{opt} \times G \tag{1.1}$$

The optical conversion efficiency is then defined as the quotient between the output of the radiative power of the light that is guided towards the edges of the waveguide structure (P_{out}) and the radiative power of the incident light on the top surface (P_{in}).

$$\eta_{opt} = \frac{P_{out}}{P_{in}} \tag{1.2}$$

The geometrical gain factor is defined as the quotient between the area of the surface (A_S), which collects the exterior radiation, and the edge area of the structure (A_{Edge}).

$$G = \frac{A_S}{A_{Edge}} \tag{1.3}$$

Due to their strong dependence, in terms of performance, with the geometry of the overall LSC structure and PV components, comparison between different devices should

be based on the values of η_{opt}, for sufficiently small areas of the waveguide structure where G suffers no significant change. [6] For scale-up, a comparison should rely on the C_G values for the LSC, which may be perceived as being a measure of the effective enlargement of the PV device, when coupled with the LSC. [17]

There are different LSC configurations where the main variance resides in the placement of the PV cell in the device. The PV cell can be coupled to the rear side of the waveguide material or it can be mounted to the edges of such structure. Regardless, they display the same potential for conversion efficiency [18]. In this work, the first configuration will be referred to as transmission geometry and the latter as luminescence geometry.

In this work the LSC structure in a luminescence geometry was composed by the combination of the host material, more specifically a Quantum Dot (QD) thin film laminated between two glass matrices, an architecture which was based in the thermochromic windows, from *Suntuitive Glass* ® [19], and the PV system, in this case a commercially available organic solar cell. In general, when describing the overall performance of these type of LSC system, one can use equation 1.4 to quantify the PV cell optical conversion efficiency, where I_{SC} and $I_{SC}{}^{L}$ are the short circuit current of the PV cell alone and the PV cell when coupled to the LSC, respectively, V_{OC} and $V_{OC}{}^{L}$ are the open circuit voltage for the PV cell alone and the PV cell when coupled to the LSC, respectively, η_{PV} is the cell's efficiency and η_{solar} is the average efficiency value of the cell with respect to the total solar spectrum. [20]–[22]

$$\eta_{opt} = \frac{I_{SC}^{L} V_{OC}^{L}}{I_{SC} V_{OC}} \times \frac{1}{G} \times \frac{\eta_{solar}}{\eta_{PV}} \tag{1.4}$$

Besides geometrical factors, the materials which compose the LSC can be finely tuned in order to further increase the efficiency of the device. However, when choosing a waveguide structure, which is composed of a host matrix embedded with luminophores, one can be confronted with a few challenges. In an ideal Transparent and Luminescent Solar Concentrator (TLSC), not only does the waveguide structure must act as a perfect light trapper but also, reflection losses at the edge of such structure should be avoided. These requirements are easily achieved making use of highly complex optical designs with antireflection coatings and 1D photonic mirrors. Nevertheless, this type of waveguide optimization would increase the cost of large scale TLSCs and add further obstacles to the implementation of these devices in the contemporary building industry. [6], [13], [23]

Today's LSCs prototypes are typically composed of Poly(Methyl Methacrylate) (PMMA), formulations of Polycarbonate (PC) or glass, since the host material needs to have

a low refractive index in order to minimize the reflectance at the front surface of the device. Even though it doesn't act as a perfect waveguide, glass is a rather customizable material, of extreme durability and with existent well-established worldwide recycling protocols, when in comparison to polymeric host materials. Furthermore, most of the market leaders associated with the building industry, and other types of industries that could make use of these luminescent devices, already have a well implemented large scale glass supply and application network [6], [11], [24].

An additional requirement, in an ideal LSC, is that the PV structure mounted around the edge of the device has an efficiency and quantum efficiency equal to the Shockley-Queisser limit. [25] This limit takes into consideration losses which limit the overall solar-to-electric power conversion efficiency [11], [26].

1.2 All-Inorganic Lead Halide Perovskite: structure and properties

Recently, perovskite materials have gained much interest due to their excellent optoelectronic properties, such as high absorption coefficients, high carrier mobility and attractive emission properties [27]–[32]. Another major advantage is their simple solution-based synthesis, which allows for easy process adaptation and industrial compatibility [29].

Trihalide perovskites follow the general formula AMX_3 (being, A= Cs^+, $CH_3NH_3^+$, $CH(HN_2)^{2+}$; M= Pb, Sn and X= Br^-, Cl^-, I^-), in terms of structure [28], [29], [31], which is displayed in figure 1.2. Crystal phase transitions can lead to a final structure such as cubic, orthorhombic or tetragonal [33], [34].

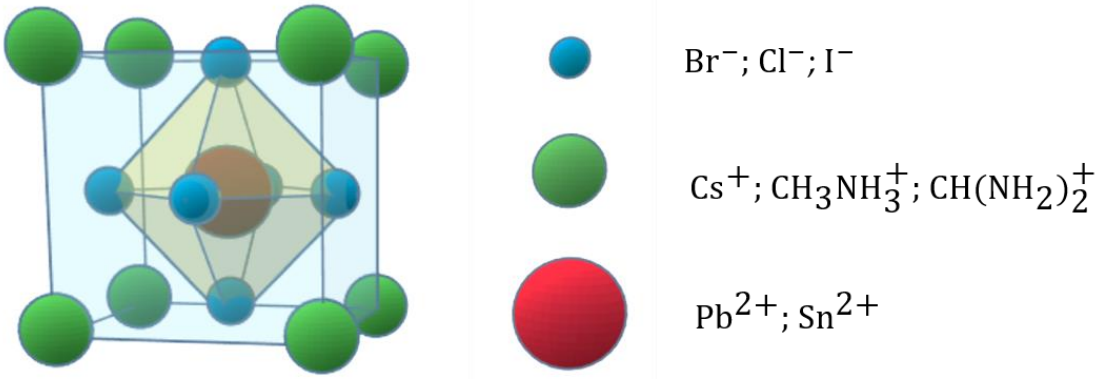

Figure 1.2: Basic trihalide perovskite unit cell structure, where the different ion radius is represented by the different sizes of the spheres, which, in turn, correspond to a certain ion.

1.2.1 Size dependence: tunable features and quantum confinment

These lead halide perovskites have an easily tunable bandgap and through dimensional control it is possible to obtain perovskite based colloidal nanocrystals, also referred to as Perovskite QDs (PQDs), which display high luminescence Quantum Yield (QY), narrow

emission peaks and emission wavelengths fully controllable through halide anion exchange and quantum size effects [28], [34]–[37].

Perovskite compounds comprise an array of supramolecular interactions whose tunability through size, shape and charge distribution of the A-site cations allied with the deformability of the host framework result in a structurally personalizable host-guest system, easily achieved through external stimuli, such as temperature and radiation [38]. These mouldable supramolecular interactions ultimately lead to easy modification of the perovskite physical properties per chemical routes [31], [33], [34], [38].

Moreover, semiconductor QDs rely on the quantum confinement effect, granting them size dependent tunability of the band gap [39]–[42]. This effect results in a discretization of the electron and hole levels, where the optically allowed transitions lead to discrete absorption bands in their UV-vis spectrum [41]. Perovskite QDs consequently show size-tunable emission wavelength together with very high and temperature-insensitive optical gain [40], [41].

Additionally, nanostructured perovskite allows for tailoring of the electronic and optical properties, through size and composition variations [39]. Colloidal perovskite QDs offer an greater quantum confinement, which results in better preservation of the emission characteristics, even at higher temperatures [39], [41].

1.2.2. LSC device compatibility

Despite of the facile deposition of the solution-based PQDs, e.g. via drop-casting or spin-coating, these rather novel materials are still facing some obstacles in terms of stability, which limits the full potential of application of these nanomaterials [28], [29], [35], [37]. Besides their poor stability, inorganic lead halide perovskites also show degradation when exposed to humidity, high temperatures, light and oxygen [28], [29], [35], [37]. These limitations can compromise the quality of the luminophore thin film that makes for the down conversion system of the LSC, consequently affecting the overall performance of the device. Allied with the lack of the device optimality, the PQDs stability may also give rise to a drawback regarding product commercialization and installation, since it can have a negative impact in the environment and safety, due to lead toxicity [37].

Since glass panels show a relatively long life-time, the Inorganic Perovskite QDs (IPQDs) need to be encapsulated to guarantee higher stability and diminish degradation, in an attempt to expand the final products durability. [43], [43], [44] Polymeric encapsulation arises as a form of protection against environmental factors, being a simple, inexpensive and industry compatible procedure [37].

M2terials and Methods

2.1. Synthesis of IPQDs: Hot-injection method

In this work, colloidal solutions of perovskite $CsPbBr_3$ QDs were synthetized using the hot-injection method, reported by Chen et al., with a further study of the influence of the final QD solution concentration. [45] For that, the pellets obtained through the chemical synthesis were re-disperse in different quantities of hexane.

All the used chemicals and precursors were purchased from different suppliers and were applied without further purifications or modifications. From *Sigma-Aldrich* were used Cs_2CO_3 (99%), Oleic Acid (90%) and 1-Octadecene (90%). From *Acros Organics*, Oleylamine (80-90%). From *Alfa Aesar*, $PbBr_2$ (98+%).

2.1.1. Cs-Oleate: preparation of the solution to be injected

Firstly, 0.4 g of Cs_2CO_3 (1.23 mmol), 1.5 mL of Oleic Acid (OA) and 15 mL of 1-Octadecene (ODE) were measured and placed inside a 100 mL 2-neck flask. The flask was then degassed under a N_2 flux, at room temperature, for 20 minutes. Afterwards, the syringe, which delivered the gas flow, was pulled back at half-height from the bottom of the flask, and the mixture was heated to 150 ºC from 1 hour to 1 hour and half, under stirring. The mixture must be fully dissolved before continuing with the hot-injection synthesis.

2.1.2. Synthesis of inorganic perovskite $CsPbBr_3$ QDs in colloidal solution

In this step, 5 mL of ODE, 0.5 mL of OA, 0.5 mL of Oleylamine (OAM) and 0.069 g of $PbBr_2$ (1.88×10^{-4}mol) were put into a 50 mL 2-neck flask, also under a N_2 flux, at room temperature, for 20 minutes. Past the 20 minutes time, the flask was heated to 120 ºC for 1 hour, with the syringe pulled back at half-height of the flask, under stirring. Then, the temperature was set to 150 ºC and the solution was left to stabilize, once it reached this temperature, for 2 to 5 minutes. In the meanwhile, the temperature of the Cs-Oleate solution was stabilized in 110 ºC and an ice-water bath was prepared, in a large enough container to accommodate the 50 mL 2-neck flask.

Once both solutions had stabilized at the right temperature, using a 1 mL syringe, 0.4 mL of the Cs-Oleate solution were injected in the 50 mL flask, which contained the remaining solution. After counting 5 to 10 seconds, still with the N_2 flux, the flask was put in the ice-water bath and left to cool. The QDs in colloidal solution were obtained after the

solution, which was injected with Cs-Oleate, was centrifuged at 5000 rpm for 20 minutes and the pellet re-disperse in hexane.

2.2. IPQDs in colloidal solution: thin film deposition and encapsulation

2.2.1. Float glass: sample preparation and deposition

In this study, perovskite thin films were deposited, from a colloidal solution, over float glasses of 3×2.5×0.16 cm. For this, the glass substrates were cleaned in a piranha solution of 1:4, using sulfuric acid (97%) purchased from *Honeywell Fluka* and H_2O_2 (35%) from *Chem-Lab,* for 1 hour and half, and their surface was activated with an UV treatment for 15 minutes, prior to the deposition. After optimization of the deposition parameters, the most uniform perovskite thin films were obtained for spin-coating depositions at 1500 rpm for 30 seconds, with a total deposited volume of 300 µL total of a mixture of a 1:2 solution of the re-disperse colloidal solution of IPQDs and a 10% wt% polyethylene-hexane solution, respectively, on the tin-comprising surface of the float glass samples. The 10% wt% polyethylene-hexane solution was made with low-density polyethylene, which was purchased from *Sigma-Aldrich*, that was mixed with the colloidal IPQDs solution to be deposited in order to adjust the solution's viscosity to obtain a more uniform thin film. Thin-films were also deposited using a 20% wt% polyethylene-hexane solution. However, the final thin film homogeneity was not as good as the one displayed by the deposited IPQDs thin films using the 10% wt% solution. The IPQDs thin films were then annealed at 50 ºC for 3 minutes. The conditions for the thin film depositions are summarized in Annex A.

2.2.2. Microcrystalline silicon PV cell: sample preparation and deposition

These µc-Si:H solar cells in a p-i-n configuration were developed in the CEMOP department from FCT/NOVA and were coated with the synthetized IPQDs and encapsulated with parylene type-C, in the same form as the float glass substrates were. Each analysed sample was comprised of a set of four individual solar cells, which for simplicity reasons will be addressed as sample A and sample B, being similar to one-another. Information on the used PV cells and IPQDs deposition parameters can also be consulted on Annex B.

2.2.3. Parylene type C encapsulation

Following the deposition, a 2 g deposition of parylene type-C with adhesion promoter, purchased from *Specialty Coating Systems*, was deposited on top of the IPQDs thin film via Chemical Vapor Deposition (CVD), using a PDS 2010 Labcoter 2 from *Specialty Coating*

Systems, Inc., in order to obtain a 100 µm encapsulation. This encapsulation was executed in order to protect the IPQDs thin film from external factors and, consequently, increase their durability and safety during handling of the samples.

2.3. Characterization

2.3.1. Optical: Absorption, emission and excitation profiles

The optical characterization of the IPQDs in solution and in thin film was preformed using absorption, emission and excitation 3D profiles of the samples in question. For the absorption measures, a quartz cell with a 1 cm optical path was filled with the diluted IPQDs solution to be analysed. The thin film samples were held in a solids support, which is an accessory of the equipment. The spectra were attained using a conventional double beam *VARIAN* spectrophotometer, model Cary-5000, from a 300 to 800 nm wavelength range.

The emission and excitation 3D profiles, of both the IPQDs in solution and in thin film, were measured in a *SPEX ® Fluorolog®-3 HORIBA* spectrofluorometer, model FL3-22. For the emission profiles of the IPQDs in solution, a quartz cell with a 1 cm optical path was used and the spectra were attained for a 460 to 470 nm range and a 465 nm excitation wavelength, with a 1 nm slit. The emission spectra for the IPQDs thin film were measured for a 440 to 550 nm range and an excitation wavelength of 430 nm, with a 0.5 nm slit. IPQDs QY was determined by the absolute method, according to standard procedure. The excitation 3D profiles were only measured for the solid samples and were attained for a 395 to 600 nm range and a 280 to 460 nm excitation wavelength range, with a 0.5 nm slit.

2.3.2. Morphological and structural: Scanning Electron Microscopy (SEM), Scanning Transmission Electron Microscopy (STEM) and X-Ray Diffraction (XRD)

For the morphological characterization, a sample of IPQDs thin film deposited on float glass, without the parylene type-C encapsulation, was coated with a 10 nm layer of gold, using a *Quorum* sputter system model *Q150T ES* from *LABOMETER*, for electron leakage purposes and its morphology was analysed by SEM using a *Carl Zeiss Auriga Crossbeam Workstation* and a *Hitachi TM3030 Plus Tabletop*.

The IPQDs in solution were also characterized in terms of their morphology, for that a STEM *Hitachi HD2700* microscopy set-up was used to gather information regarding particle size, distribution and morphology. To complement the STEM results and to perform a structural study of the IPQDs in solution, XRD analysis was executed in a drop-cast sample in a silicon wafer substrate that was left to air-dry in order to evaporate the solvent present in the colloidal solution. The scan analysis was performed using a *PANalyticalX'Pert Pro* X-

ray diffractometer, with a copper anode material, in a PW3071/xx Bracket sample stage. Measurements were carried out from a 10^{o} to 90^{o} (2θ) range and the spectrum was acquired with a *High Score Plus* software.

2.3.3. Electrical: Spectral response and I-V curve

A 3D structure, which was design in *Tinkercad* software to resemble a window frame, was used to support the TLSC (Transparent and Luminescent Solar Concentrator) coupled to an organic PV module, only at one edge of the structure. The PV module was purchased from *InfinityPV* ®, in tape form. [46] The overall TLSC plus 3D frame structure, together with the LSC device in transmission geometry coupled to an organic solar cell, were characterized through the measurement of I-V curves using a *Newport-Oriel* ® *Instruments LCS-100* solar simulator, together with an *Oriel* ® *Instruments* software. The External Quantum Efficiency (EQE) spectra, which compares the response of the organic PV module to the AM1.5G solar spectra was attained using an *Oriel* ® *Quantx300* equipment, together with an *Oriel* ® *Instruments* software.

The electrical characterization of the transmission geometry comprising the µc-Si:H PV cells was executed by means of I-V curves, obtained using an *Oriel* ® solar simulator filter AM1.5G, model 2 LED Class AAA, together with an *Oriel* ® *Instruments* software. The spectral response of the µc-Si:H cells samples was also obtained, using a *Newport-Oriel* ® equipment, model *Quantx300*, together with an *Oriel* ® *Instruments* software.

Re3ults and Discussion

3.1 LSC and TLSC: design and characterization of the devices

A fundamental study was conducted where the two available LSC geometrical configurations, which are displayed in figure 3.1, were developed with the vision to optimize the amount of light that is harvested and converted through a solar cell. Keeping in mind the ultimate goal of integration of these devices in BIPVs, some considerations were applied to the development of all of the devices and prototypes.

For building integration, the acceptable visible transmittance for comfortable building application ranges from 30 to 63%, depending on the geographical localization of the construction. [44], [47]–[50] The visible light range is the only determinant, radiation wavelength wise, since it is the only one to be perceptible by the human eye. [51], [52]

For environmental and durability purposes, the chosen host matrix material was soda-lime-silica or float glass. Besides being widely available, it is extremely used in the construction industry and it can be obtained from waste products as well as recycled to originate new products and materials. [53]–[55] Research investigation with LSCs and TLSCs has found many obstacles associated with the use of float glass as the waveguide material, however, being a rather cheap and recyclable material, this work focuses on the implementation of this material in the developed LSC and TLSC devices.

For product implementation, safety measures and long-term stability, the $CsPbBr_3$ IPQDs were encapsulated with parylene type-C. This prevents the leakage of solution from the devices, while theoretically expanding the IPQDs lifetime to better match the one of the host matrix material. [56]–[59]

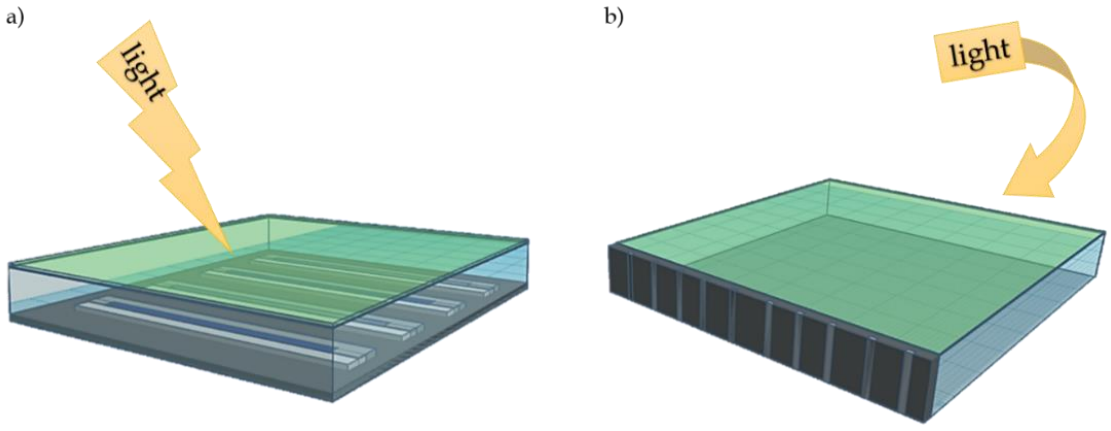

Figure 3.1: LSC geometrical configuration being a) Transmission Geometry, where the light hits the host matrix surface and the PV component is located on the rear host matrix surface, and b) Luminescence Geometry, where the light hits the exposed host matrix surface and the PV component is located on the edge or edges of the device.

3.1.1. Transmission Geometry: design and components

Host matrix material

In an initial stage of this project, one of the host matrix materials to be studied was a soda-lime glass doped with europium luminescent species, instead having them deposited on top of the inorganic substrate. However, it has some drawbacks, since its synthesis at lab scale is rather lengthy and difficult to scale-up to large dimensions, such as 10x10 cm. Afterwards, the used glass substrates were obtained from large float glass panels, which were cut into smaller 2.5x3 cm samples and whose edges were carefully polished in the laboratory, in order to avoid light scattering in the waveguide structure. These samples worked well in preliminary tests. However, the float glass substrates still showed many macro and micro scratches. It was decided to avoid the presence of these random defects by purchasing float glass samples from *Vidreira Infante, Lda.*, with the same dimensions of 2.5x3 cm and already polished edges.

As it was mentioned before, the chosen material for the host matrix was soda-lime-silica glass. There are many disadvantages associated with the use of this material for a waveguide structure, however, there are many advantages linked to this material, both in terms of physical and optical properties of the material along with its recyclability. Besides its recyclability, when in comparison to polymeric materials, glass matrices have a more direct application approach, that is, they do not necessarily need to rely on the employment of UV-stabilizers nor additives, which can ultimately reduce the overall performance of the device. [60] Regarding its physical and optical properties, float glass meets the demands needed for the efficient design and implementation of both a LSC or a TLSC. Its refraction index is rather close to the required refraction index in a LSC, being $n_{float} = 1.52$ [61], thus minimizing reflectance losses at the front surface of the device and still being able to perform TIR of the visible fluorescent emission from the luminophores. [12], [62]–[64]

Another major requirement for the host matrix material, knowing the application in BIPV, it is the transmittance of such material. As referred earlier in the chapter, a specific visible transmittance between 30 and 63% is desired, depending on the location of the construction site. With the use of float glass, it was possible to obtain a maximum transmittance of 86%, with an average value of 84% in the visible range, for the float glass alone, and 64%, with an average value of 52% in the visible range, with the incorporation of the IPQDs, as it is seen in figure 3.2.

Additionally, for LSC manufacturing purposes, it is required that the host matrix material is compatible with the processing temperature ranges, being those, in this case, the annealing temperature of the luminophore thin film and of the protective encapsulation of the IPQDs. [63], [64], [66]

The used float glass has a glass transformation temperature of 500ºC to 580ºC and given that the IPQDs thin film annealing temperature does not exceed the 60 ºC and that the encapsulation is performed in ambient temperature, there is utterly compatibility with the processing temperature ranges. [67] Furthermore, regarding the thermal stability and durability when exposed to external environmental conditions, float glass exhibits great properties, being widely used in architecture, automotive and solar harvest and conversion systems. [68] This offers a major opportunity for easy and lower cost implementation of float glass based LSCs and TLSCs.

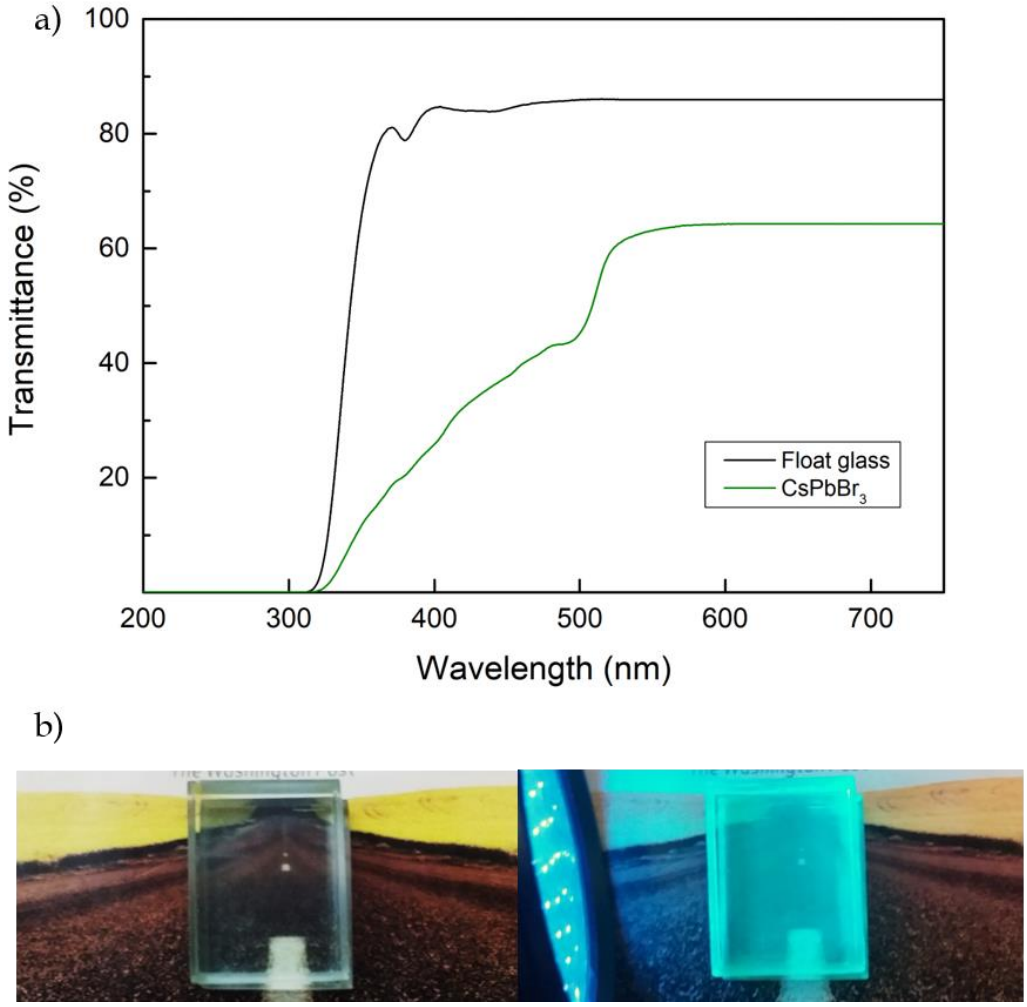

Figure 3.2: Optical transmittance when a) the analysed sample is irradiated with light of the UV-visible range and b) when the IPQDs sample is irradiated with an UV-length only light source.

$CsPbBr_3$ IPQDs as luminophores and its' encapsulation using parylene type C

Luminophores are a huge component of LSCs and TLSCs, since they provide the optical properties necessary for the absorption of incident radiation and its conversion, thru down-shifting or up-conversion, to higher or lower radiation wavelengths, in order to better enhance the performance of the coupled PV device. [60], [65]–[67] For efficient LSC or TLSC application, there are several factors inherent to the chosen luminescent species.

The absorption of the incident radiation must be significant and the absorption needs to decrease sharply to zero near the bandgap, were the PV system has the maximum harvest and conversion efficiency of light. [23], [68], [69] However, efforts to increase the overall absorption of the luminophores, for example by increasing its concentration, lead to an increase in the loss mechanisms due to self-absorption of the emitted light, which is already one of the major causes of poor efficiency in large scale LSC devices. [60], [67]

The luminescent quantum yield needs to be sufficiently high (in an ideal case close to or equal to the unity) since it has direct effect in the optical efficiency, that is, the ratio between the number of photons that reach the waveguide edge and the number of photons incident on the waveguide surface. [23], [68], [70]

Regarding the final application of the luminophores on the host matrix, it is desirable, in some cases, that the luminescent species shows some solubility in the waveguide material. [23], [68] Higher photostability can be of major interest depending on the final device application. [23], [60], [68] Allied to the loss mechanism through reabsorption of the emitted light, the Stokes Shift, that is the separation between the absorption and photoluminescence emission profiles of the luminescent species, needs to be as high as possible in order to diminish this effect. [18], [23], [60], [66], [68], [71]

As discussed in the introduction chapter, the chosen luminophores for development of this work are a rather recent approach, comparatively with the traditional luminescent dyes for LSC applications. The IPQDs offer many advantages over the organic or inorganic dyes due to their tunable optical properties, higher luminescent QYs and short radiative lifetimes. [30], [35], [72]–[74] In a first approach, both $CsPbBr_3$ and $CsPbI_3$ IPQDs were synthetized. The idea was to proceed with the implementation of the $CsPbI_3$ QDs in the final LSC and TLSC devices, due to better matching of the bandgap of these iodine spiecies with the maximum of efficicency of both the amourphous sillicon and organic PV module.

However, the synthetized $CsPbI_3$ QDs showed to be very unstable and demonstrated fast degradation, in comparison to the $CsPbBr_3$ QDs. Since further otimization of the IPQDs synthesis together with the development and application of protective shell doping were not feasable for the project duration, the study of the LSC and TLSC comprising devices was conducted with the use of the $CsPbBr_3$ QDs.

The synthetized $CsPbBr_3$ QDs were analysed and the obtained absorption and PL emission spectra are displayed in figure 3.3. As expected, the synthetized IPQDs show a broad band absorption with a well-defined excitation transition peak, has reported in literature. [72]–[75] However the presence of other excitation peaks near the 460 nm, in the colloidal solutions of re-dispersed pellet in 10 mL and 5 mL of hexane, suggest non-uniformity of the morphology and size of the synthetized IPQDs. [72] Also, the excitonic absorption peak is more prominent in the 10 mL and 5 mL re-dispersions than in the 2.5 mL one, which might indicate that the majority of the IPQDs present in the first solutions may have a monoclinic crystal structure while the latter ones, in the higher concentration solution, may display a higher population of cubic structured IPQDs. [74] These structural, morphological and size dependent factors were further investigated by means of STEM imaging and XRD analysis and the results are discussed later in this chapter.

Regarding the PL emission spectra, also displayed in figure 3.3, it is observable that there is not any significant variation of the emission intensity, when comparing solutions with different concentrations. However, there is a slight red-shift with the increase in the IPQDs concentration in solution, from 495.7 nm, in the case of the re-dispersed pellet in 10 mL of hexane, to 497.2 nm, for the re-dispersed pellet in 5 mL of hexane, and all the way to 500.5 nm, for the highest concentration solution. Absorption and emission red-shifting is, normally, noticeable in size variations or aggregation of the particles present in the colloidal solution. [30], [72], [73], [75]–[77]

All the PL emission spectra show bell-shaped symmetrical forms. Nonetheless, PL emission spectrum for the pellet re-dispersed in 2.5 mL of hexane exhibits a slight discrepancy of heights for the lowest emission values, from a mixed Gaussian and Lorentz asymmetric profile. This might indicate the existence of defects in the surface of the synthetized IPQDs or the presence of contaminant luminescent species, at much lower concentrations that those of the synthetized IPQDs, probably derived from a structural phase transition or from contamination of the used quartz cell. [78], [79]

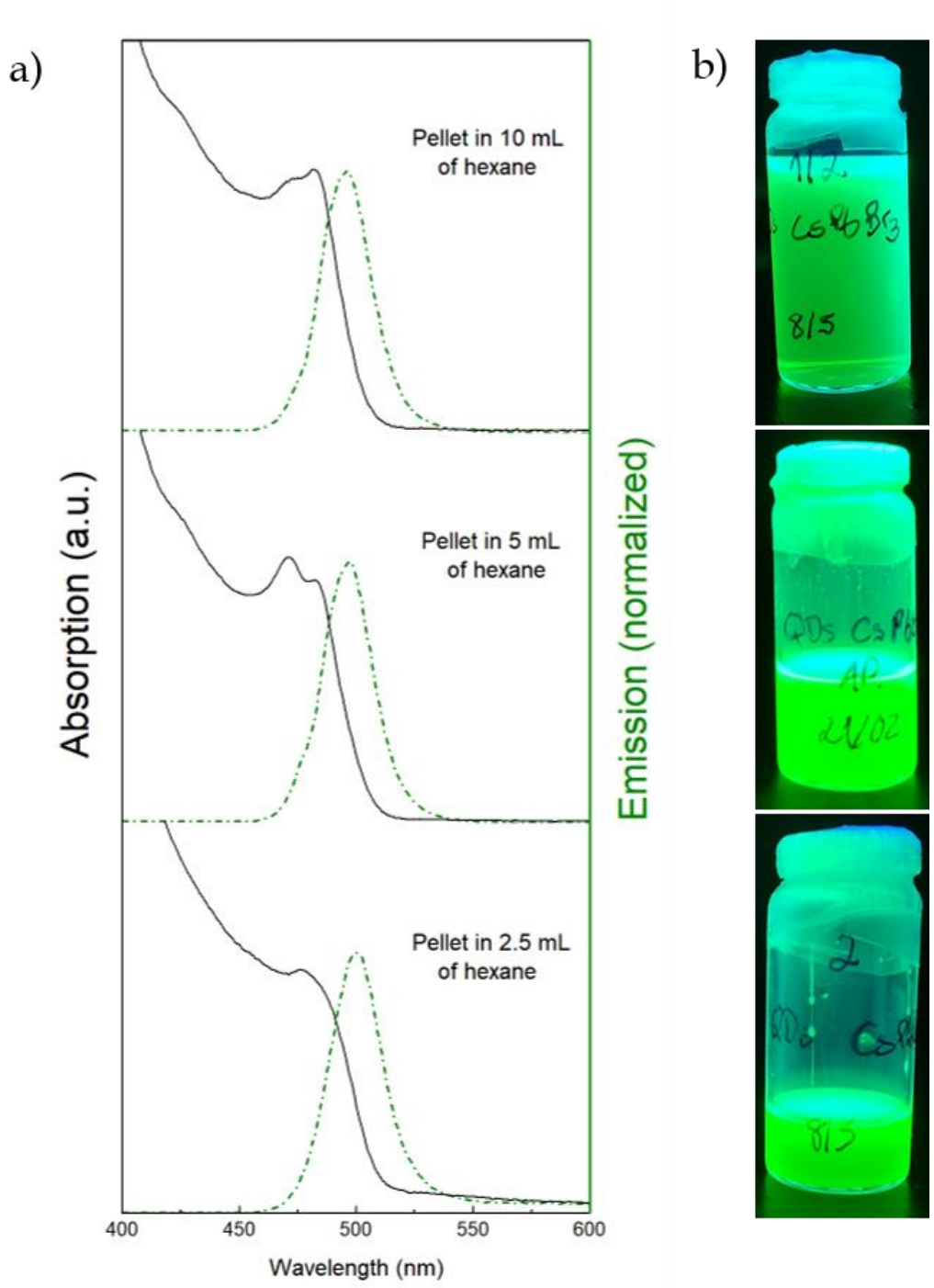

Figure 3.3: IPQDs in solution where a)UV-vis absorption and emission spectra, with a 445 nm excitation wavelength, of the re-dispersed IPQDs pellets in different amounts of hexane (10 mL, 5 mL and 2.5 mL for a top to bottom view), leading to colloidal solutions with different final IPQDs concentrations and b) Physical appearance of the IPQDs solution, in respect to each concentration displayed (each image corresponding to the mentioned concentration on the left spectra), when irradiated with a 365 nm light source.

The STEM images and XRD analysis corroborate, in fact, the presence of IPQDs resultant from a structural phase transition from the original synthetized $CsPbBr_3$ QDs and this finding is further discussed in this chapter, along with the STEM images and XRD data. SEM imaging analysis was also performed. However, it was not possible to obtain good

quality images of the synthetized IPQDs, since the resolution limit of the equipment was not enough to visualise the smallest colloidal species present in the sample. Also, SEM imaging of the larger size species was inconclusive due to the presence of very large impurity sites, since the final colloidal IPQDs solution was not washed nor purified for the acquisition of these images.

The EQE was measured for the synthesized IPQDs, by means of the absolute method using an integrating sphere, for the highest concentration solution, since the final LSC and TSC devices were manufactured using replicas of this colloidal solution, due to the better enhancement of the overall device efficiency through higher luminophore concentrations, to a certain extent. [75], [80]–[83] The analysed QDs exhibited a 68% EQE, which is in accordance with the values presented in literature for chemical route synthesis via the hot-injection method. [41] The obtained absorption and emission profiles used in the calculation of the EQE for the IPQDs in solution can be found in Annex C.

The data and images displayed in figure 3.4 were obtained from the structural analysis, by XRD, and from the morphological examination, through STEM, of a higher concentration and a lower concentration sample, respectively. The XRD data shows a very intense signal around 15 ^{o} and 30 ^{o} with correspondence with the (100) and the (200) facets, meaning that the cubic phase species are arranged with the same spatial orientation.

In the STEM image, displayed in figure 3.4 c), it is observable and distinguishable, the presence of at least three entities of different size and morphology. Together with Annex D, which displays a larger sample area giving a better landscape of the IPQDs quantities and distribution, it is clear the presence of Nanoplates (NPLs). Nevertheless, they constitute a minority relatively to the other species present. These nanoplates might be an indicative of the existence of cubic $CsPbBr_3$ perovskite structures, which through post-synthesis dilution and ambient exposure during ageing of the colloidal solution result in the formation, to a low extent, of bigger 3D and 2D anisotropic structures. [84] Furthermore, these morphological and structural changes, often induced by moisture, light and air exposure, result in bigger anisotropic structures, usually of larger lateral size, with a clear orthorhombic Pnma phase. These nanoplates can also arise from superstructures of the $CsPbBr_3$ building blocks which form linear chains of preferential crystallographic orientation and well-established long-range order, also referred to as mesocrystals, which assemble into stacked columnar phases in higher NPLs concentrations. [85], [86]

Nanoplates can also adopt a different arrangement into large 2D sheets formed by lateral crystallographic attachment of single plates. Both these NPLs arrangements are visible in the STEM images of figure 3.4 and Annex D.

There is a visible contribution of all the major peaks' correspondent to the $CsPbBr_3$ cubic and orthorhombic phase structures, represented in figure 3.4 by the larger size black asterisks. However, from the XRD data and STEM images alone, it is not possible to conclude whether these contributions arise from the presence of either a cubic $Pm\bar{3}m$ structure, an orthorhombic Pnma structure or both these structures. Nevertheless, the presence of three distinguishable lower intensity peaks, marked with the smaller size green asterisks, may be an evidence of the presence of the orthorhombic Pnma structure in this specific higher concentration sample, which is the expected thermodynamically stable crystal phase structure at room temperature. [84] Unfortunately, the STEM images alone, cannot be used to differentiate the orthorhombic from the cubic structures since, even with the possibility of identification of the smaller structures d-spacing, both these phases exhibit similar interplanar distances. [87]

The XRD analysis also shows the presence of a rhombohedral structure, which is also visible in the STEM images taken for the same higher concentration sample. This arises because a phase transition from a 3-dimentional $APbX_3$ perovskite to a 0-dimentional A_4PbX_6 perovskite occurs. [88], [89] It is possible that these hexagonal superlattices are a consequence from the self-assembly and agglomeration of the $CsPbBr_3$ NPLs present in low-Pb composition solutions, which are quantum confined metastable species due to their small vertical dimensions in comparison to their lateral size, giving rise to a thermodynamically favoured polymorph of rhombohedral phase structure. [90] Further study of these 0-dimension perovskite structures might be of great interest regarding the final LSC and TLSC applications, since these species display longer structural stability in comparison to the cubic and monoclinic crystalline phases in ambient conditions. [84] Additionally, these rhombohedral structures also exhibit higher luminescence QY than the $CsPbBr_3$ variants, whose presence in solution as an impurity element renders lower luminescence QY of the solution and broader FWHM of the PL spectra, when comparing the luminescence QY of the colloidal solution versus the thin film. [89]

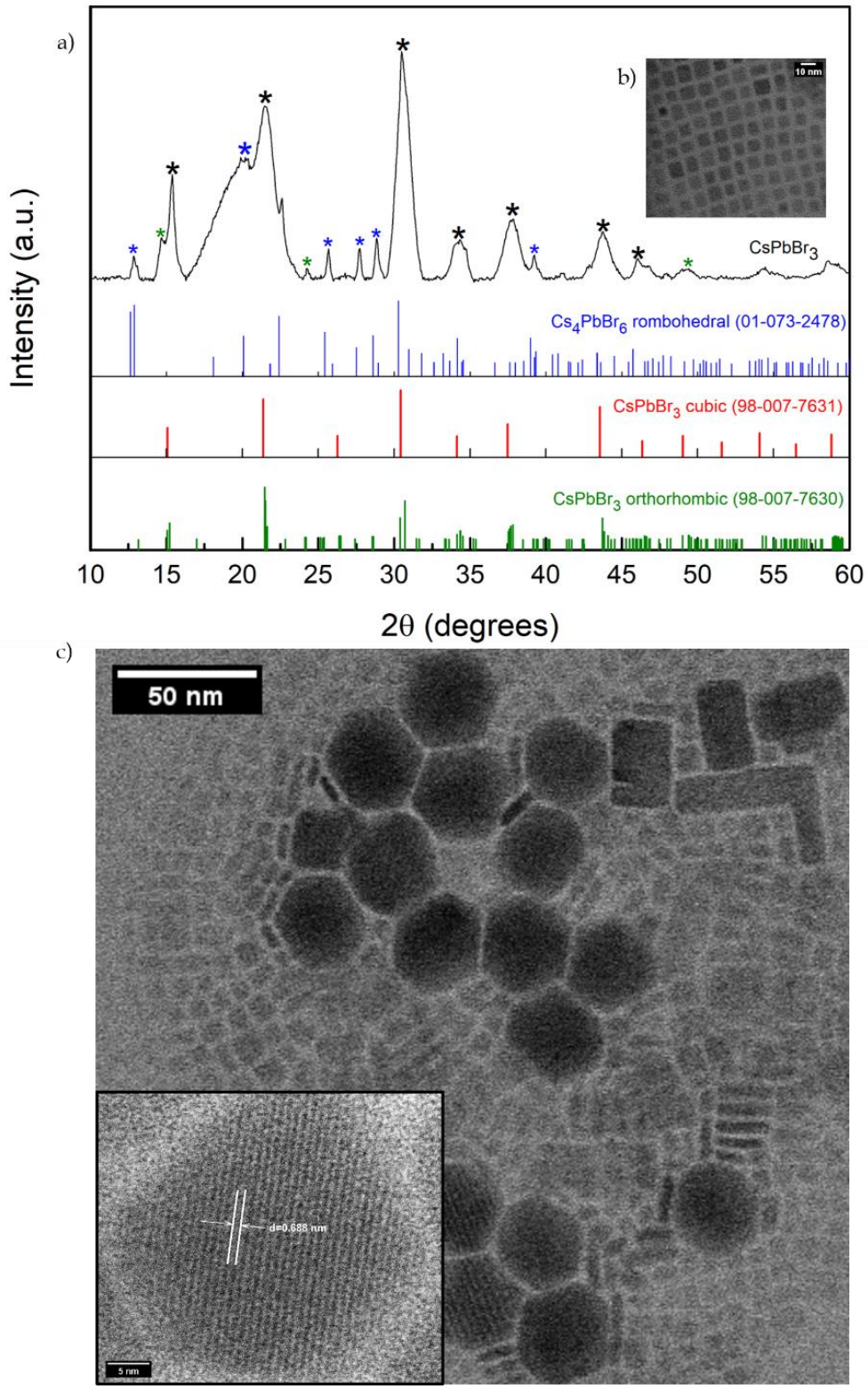

Figure 3.4: Structural analysis where a) is the collected X-ray diffraction data of a drop cast from the higher concentration solution (pellet re-dispersed in 2.5 mL of hexane) in a quartz substrate, along with the XRD patterns for $CsPbBr_3$, both the cubic (ICSD ref. 98-007-7631) and the orthorhombic (ICSD ref. 98-007-7630) crystal phase, and Cs_4PbBr_6, with a rhombohedral crystal phase (ICSD ref. 01-073-2478). Morphological analysis where b) is a STEM image of the rearrangement of the cubic or orthorhombic phase IPQDs and c) is a STEM image of a section of the sample in which is notable the presence of nanocubes, nanoplates and octahedral IPQDs. The bottom STEM image in sub-figure c) shows an isolated rhombohedral IPQD with clear lattice fringes and an estimated interplanar distance of 6.88 Å.

Together with the XRD data and STEM images, the presence of very small absorption peaks localized near the 220 nm and 313 nm range, for the absorption spectrum of the highest IPQD concentration colloidal solution (see in Annex E), can be attributed to the minority population of hexagonal Cs_4PbBr_6 platelets. [88], [91] Their presence can explain the shift in location of the PL emission peak, from the obtained peaking at 500 nm to the 510-520 nm emission peak reported in literature for the $CsPbBr_3$ nanocrystals. This shift arises from the contribution of the $CsPbBr_3$ NPLs, which provoke a blue shift of the PL spectrum, with an emission peak centred from 405 nm to 488 nm, depending on the thickness of the perovskite unit cell. [86], [92]–[94]

The 3D PL plots for the colloidal IPQDs thin film depositions were obtained and, as displayed in figure 3.5, the excitation wavelength which leads to greater emission intensity is centred at 290 nm, with a correspondent emission peaking at 480 nm, for both the one-deposition and the two-deposition thin film sample, encapsulated with parylene type-C via CVD. It is also noticeable an increase in intensity for the two-deposition thin film contour plot, as expected using the same acquisition parameters in the experience. The 3D spectra do not show any secondary emission maps, pointing out that the luminescence arises from a "single-species". The 3D PL contour plot of the emission *versus* excitation wavelengths for a blank sample of a float glass slab encapsulated with type-C parylene is displayed in Annex F, for reference purposes.

All inorganic perovskite QDs show high compatibility with LSC and TLSC integration, due to their facile synthesis through wet chemistry approaches, high QYs, size-tunable absorption and emission spectra and better chemical and photo-stability in comparison with organic dyes and polymers. [14], [47], [95]–[98] Regarding process compatibility, the variety of chemical-route synthesis available in literature, either by hot-injection method or room-temperature synthesis, guarantees the versatile processing and reproducibility of the IPQDs in colloidal solution. Furthermore, the facility to adapt the colloidal IPQDs solution deposition, employing either spray-deposition or dip-coating deposition methods, instead of a spin-coated deposition, allows for the application of these thin films in inorganic glass substrates, ranging from small to large scale areas. In terms of the overall life-time of the final device, either in transmission or luminescence configuration, additional testing is needed in the future in order to quantify the photo and thermal stability of the synthetized IPQDs, along with performance evaluation and product life-time assessment of the final LSC and TLSC devices in external environment conditions.

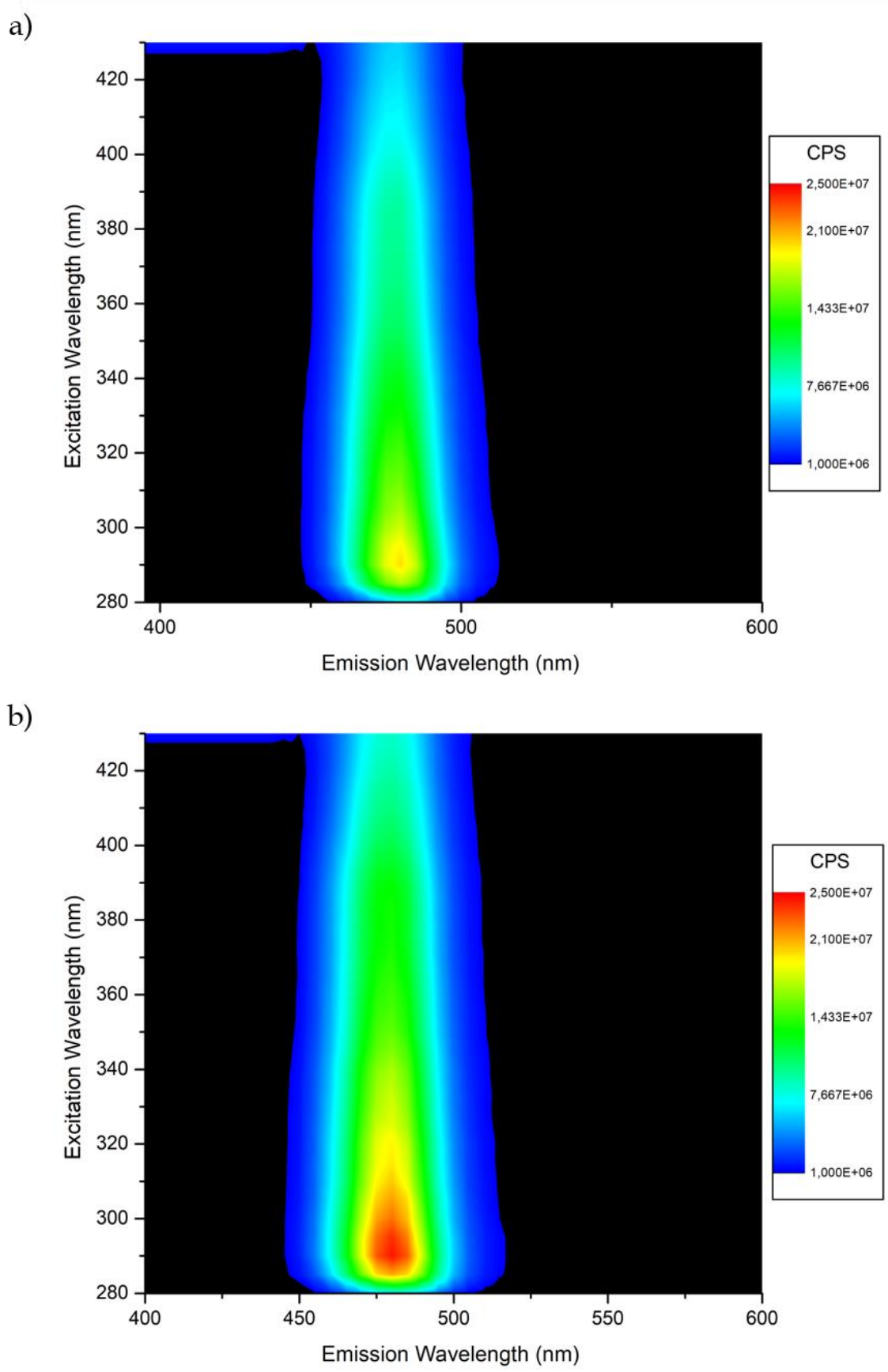

Figure 3.5: 3D Photoluminescence contour plots (emission *versus* excitation) of a) a one-deposition thin film sample of spin-coated float glass slab with IPQDs, encapsulated with type-C parylene and b) a two-deposition thin film sample of spin-coated float glass slab with IPQDs, encapsulated with type-C parylene.

All inorganic perovskite nano-crystals, like hybrid-perovskite nano-crystals, show high sensitivity to moisture and oxygen. [14], [97], [99] Therefore, in an effort to avoid leaking of lead in the handling of the device and to reduce degradation of the luminophores, consequently increasing the devices lifetime, an encapsulation with parylene type-C is employed over the deposited colloidal IPQDs thin films. Parylene type-C is one polymeric coating of the *Parylene series* from *Specialty Coating Systems*, with a modified form from the raw materials dimer, Parylene N, by substitution of one of the aromatic hydrogens with a chloride atom. [100] Since parylene type-C was deposited via CVD, the application of this polymeric coating leads to a reduction in the amount of reflected light at the parylene-air interface and thus to an increase in transmittance, consequence of the reduction in rugosity of the colloidal thin film surface. This justifies the increase in the PCE for the μc-Si:H PV cells, in the transmission geometry, comprising the IPQDs layer, in the 433 nm to 542 nm range for one sample and in the 475 nm to 611 nm range for the other sample, as it is shown in sub-chapter 3.1.3. In the luminescence geometry, the increase in the PCE values for the organic PV cells are also justified by the presence of the parylene coating, together with the waveguide behaviour of the used glass substrates.

In every executed measure, the adding of the parylene type-C coating has helped to improve the obtained results. For example, as seen in figure 3.6, and comparatively with figure 3.2, the maximum transmittance values show an increase in number to 88% for the float glass encapsulated with a parylene type-C thin film and 79% for the float glass coated with IPQDs and encapsulated with a parylene type-C coating. The average visible transmittance values also show an improvement, from 84% to 83% for the float glass encapsulated with parylene type-C and from 52% to 75% for the float glass coated with IPQDs and encapsulated with a parylene type-C coating.

This polymeric coating is of easy integration as a LSC or TLSC encapsulation component, since it is deposited via CVD, which is easily scaled-up. Furthermore, parylene shows great thermal, physical, mechanical and optical properties, together with barrier function towards water and low gas permeability, which makes this type of polymer suitable for IPQDs encapsulation. There are four types of parylene coatings which belong to the *SCS coatings Parylene series* and, from this series, both parylene type-C and parylene HT show good properties for LSC or TSC integration, such as high transmittance in the visible range. However, parylene type-C is not suitable for long-term UV light exposure and, even though parylene HT outlines this problem it shows much bigger permeability to oxygen than the parylene type-C coating.

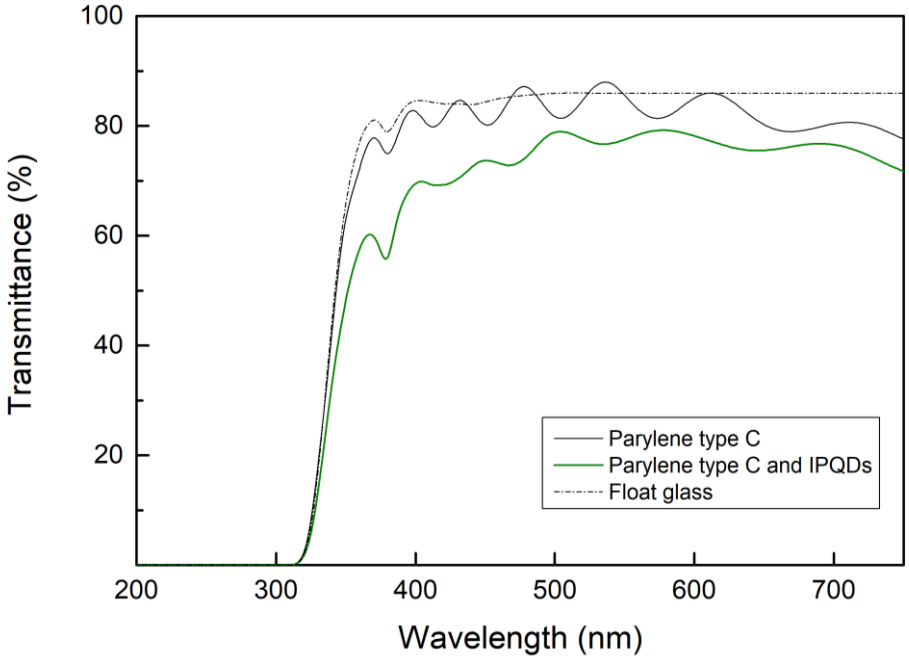

Figure 3.6: Transmittance of both float glass encapsulated with a parylene type-C coating, float glass coated with IPQDS and encapsulated with a parylene type-C coating and float glass substrate without the polymeric encapsulation. The graph shows an interference pattern present from the 400 to 750 nm wavelength range originated by the parylene type-C thin-film coating.

Comparison between the absorption peak, PL emission peak and FWHM (Full Width Height Maximum) of both the IPQDs in colloidal solution and in thin film can be observed in table 3.1. The comparison of the obtained experimental values shows that there are not big discrepancies regarding the bandgap and FWHM for the IPQDs, both in colloidal solution and in thin film. However, the emission peak suffers an approximated 20 nm blue-shift when in thin film with the polymeric encapsulation. This result can be explained by the presence of the parylene type-C polymeric coating, which contains a chloride atom in its aromatic ring. Perovskite nanocrystals have an instable crystalline structure and substitution of the halide in this structure is feasible and it can take place in a dynamic fashion. [101]–[103] Thus, the emissions peak blue-shift upon the presence of the polymeric coating leads to the deduction that there has occurred an anionic exchange, to a certain degree, of some of the bromide for chloride anions.

Table 3.1 also gives a better insight of the luminescent behaviour of the synthetized IPQDs samples. Conclusively the bandgap suffers little variation from the colloidal solution to the thin film, indicating that there is not a significant alteration of the dimensions and morphology of the luminescent species post-deposition and encapsulation. The smaller bandgap exhibited by the IPQDs in the thin film can be explained by a partial substitution of the bromide by a chloride, resulting in a slight blue-shift of emission peak for all the

samples that contain the polymeric encapsulation (see Annex G). This blue-shift is also noticeable visually under a UV-lamp, with a variation from a green emitting thin film to a blueish one, post-encapsulation of the IPQDs coating.

Table 3.1: Bandgap, FWHM and PL emission peak of both the IPQDs in colloidal solution and in thin film.

	Bandgap (eV)	FWHM (nm)	λ_{PL} (nm)
IPQDs in colloidal solution	2.42	27.5	500.1
IPQDs in thin-film *the PL associated results were obtained from samples encapsulated with parylene type-C	2.34	27.3	480.3

Coupling with organic solar cell

An organic solar cell was used in order to assess the electrical performance of the developed LSC and TLSC, both in the transmission and luminescence configuration. The used solar cell is commercialized in a tape form and, for this type of LSC geometry, the already coated and encapsulated IPQDs glasses were put on top of one of the *InfinityPV* ® solar modules and the electrical characterization was posteriorly conducted. Information regarding the comparison between the cell's spectral response and the AM1.5G solar spectra, can be consulted in Annex H.

Coupling with µc-Si:H solar cell

For a different transmission configuration study, two samples of µc-Si:H p-i-n PV cells were coated with the synthetized IPQDs and encapsulated with parylene type-C, without further modification to the 4-cell sample set in order to evaluate the electrical behaviour of the same LSC concept in an alternative and more efficient PV device. Information regarding the comparison between the cell's spectral response and the AM1.5G solar spectra, can be consulted in Annex I.

3.1.2. Luminescence Geometry: design and components

TLSC components

The TLSC components used for the luminescence geometry are the same as those used for the transmission geometry, with a modified set-up and an additional 3D structure that accommodates and secures the overall device. This 3D printed structure is better described in the next section of this sub-chapter.

3D window frame structure

For the luminescence geometry, a 3D structure resembling a window frame was printed, in CENIMAT, in order to accommodate the developed TLSC device, alongside with the integration of the organic PV module in the overall system. The designed structure is displayed in figure 3.7, together with a picture showing the bottom opening of the assembly, where the PV module is to be coupled and held with the remaining structure, whose recesses fit onto those present in the bottom part of the frame structure.

After printed, the inside of the 3D structure was carefully covered with aluminium tape, to ensure the smoothest coverage possible. This aluminium covering is used to reflect the light that reaches the edges of the device, that are not coupled to a PV module, back into the waveguide structure, hence preventing further optical losses associated with the assembly of the overall TLSC device. The figure present in Annex J gives insight on the performance of the aluminium covering as a reflective material in this window frame configuration.

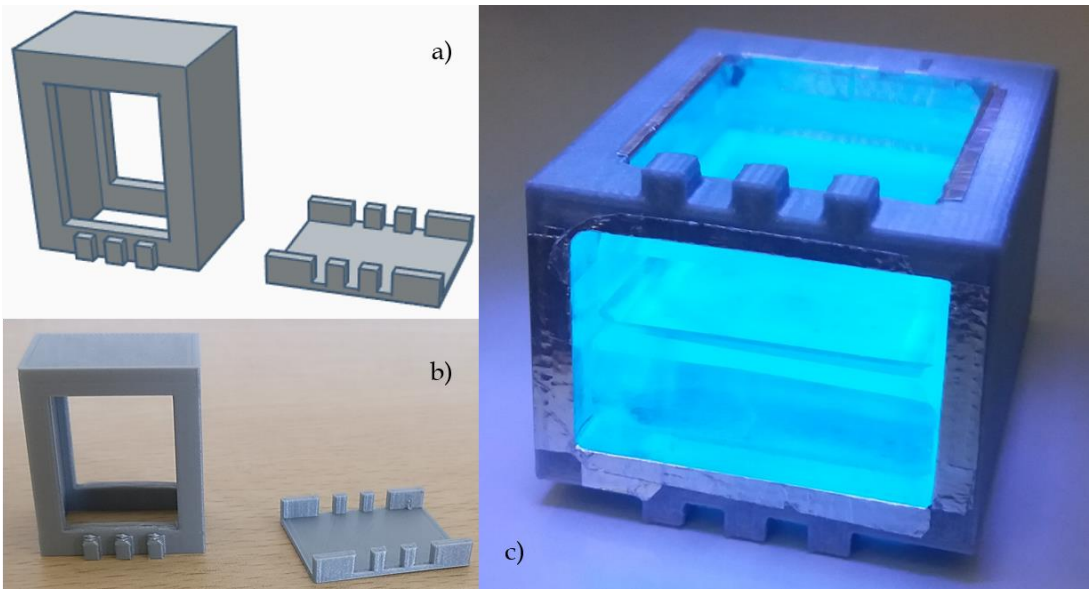

Figure 3.7: 3D printed window frame like structure where a) displays the design in the *Tinkercad* software, b) shows the structure in the physical form and c) demonstrates the accommodation of the IPQDs coated and parylene type-C encapsulated float glasses in the final structure, with the inside already covered in aluminium tape.

Due to the assembly of the glass samples and the internal coverage with aluminium tape, this structure mimics the overall structure of commercially available float glass windows, usually having an aluminium framework to hold a simple laminated glass panel. This gives us insight of the performance of these TLSC systems, not only has laboratory prototypes, but also has functional windows for building integration in the future.

3.1.3. Devices characterization

Electric characterization: Transmission Geometry

In comparison to the obtained I-V curve when the µc-Si:H PV solar cell is irradiated with 1 Sun, the organic PV solar cell in the transmission geometry together with the float glass substrate, that contains only the IPQDs deposition, shows a decrease of its current density and voltage values, as seen in figure 3.8. This happens because this configuration is more susceptible to optical losses in the edges of the waveguide structure, since the light is not being re-directed towards the glass by a reflective coating or mirror. However, the measured I-V curve for the float glass sample with parylene type-C, which contains the IPQDs deposition together with the 1 µm parylene type-C encapsulation, shows a slight increase in both the values of the current density and voltage. Such increase can be explained by the optical properties of the polymeric coating.

Since the coating is present both in the top surface and on the edges of the float glass and reduces the overall rugosity of the deposited colloidal thin film, the incident light on this parylene-air interface is less reflected than if the polymeric coating was absent, as it is corroborated by the transmittance spectra displayed in figures 3.2 and 3.6. Also, due to the differences in the refraction indexes of the Indium-Zinc Oxide (IZO) and µc-Si:H layers of the µc-Si:H PV cell, light that is transmitted to the µc-Si:H layer, beyond a specific angle,

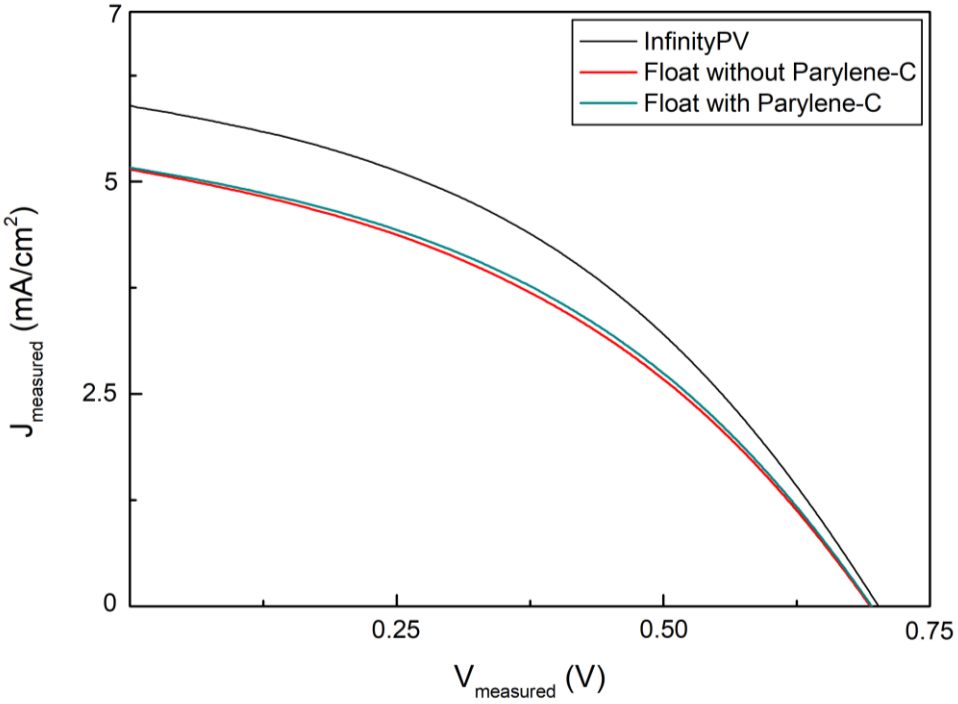

Figure 3.8: Measured I-V curve of only the *InfinityPV* ® tape and of the LSC samples, coupled to the *InfinityPV* ® tape, with and without the polymeric encapsulation. All the measures were performed under a 1000 W/m² of incident radiation, in normal with each one of the devices.

will suffer TIR at the IZO-microcrystalline silicon interface. The refractive index of the IPQDs is neglected in these calculations due to photoinduced changes related with its value. [104], [105]

Accounting for the optical losses at the edges of the LSC device and increasing the IPQDs concentration in the deposited film, leads to the conclusion that is possible to surpass the current density and voltage values measured for the *InfinityPV* ® tape alone. Table 3.2 displays the values for the optical efficiency, glass efficiency and transmittance efficiency, showing an increase in the calculated optical efficiency, when comparing the float glass substrate with the developed LSC.

The measured I-V curves for the transmission geometry using an µc-Si:H, present in figures 3.9 and 3.10 for similar samples, demonstrate a rise in both the current density and voltage values, posteriorly to the coating with the IPQDs. These values also surpass those of the measured for the PV solar cells, before any alteration to the device was performed. The Power Conversion Efficiency (PCE) values for the sample A are of 5.08% for the sample without the IPQDs deposition and 5.25% with the IPQDs deposition. This can be explained by the geometry of the samples, since the IPQDs are deposited directly on top of the µc-Si:H cells and posteriorly encapsulated with the polymeric thin film, there will be more transmitted light across the parylene layer to be absorbed by the luminophores and emitted

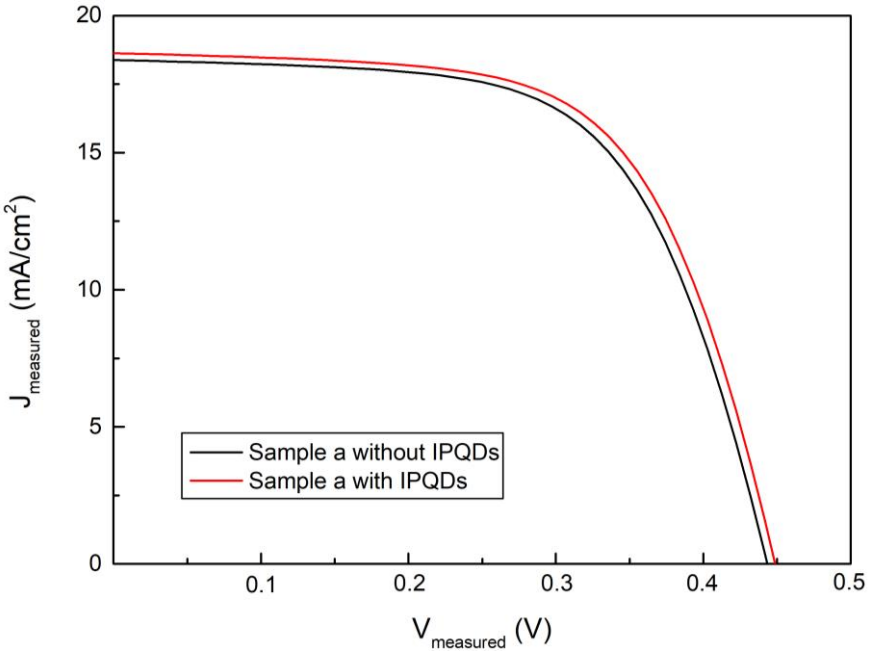

Figure 3.9: Measured I-V curve the LSC device, which comprises the µc-Si:H PV cells with and without the IPQDs coating and the polymeric encapsulation. The represented sample is a set of four individual µc-Si:H PV cells and the demonstrated I-V curves were obtained from the individual cell that better describes the performance of the cells present in the sample. All the measures were performed under a 1000 W/m^2 of incident radiation, in normal with the front surface of each PV cell sample.

directly towards the PV solar cell. Sample B also demonstrates a rise in the PCE values after the IPQDs implementation, from 4.69% to 4.91%, however is of lower variation in comparison with sample A, due to irregularities associated with the thin film cell deposition itself.

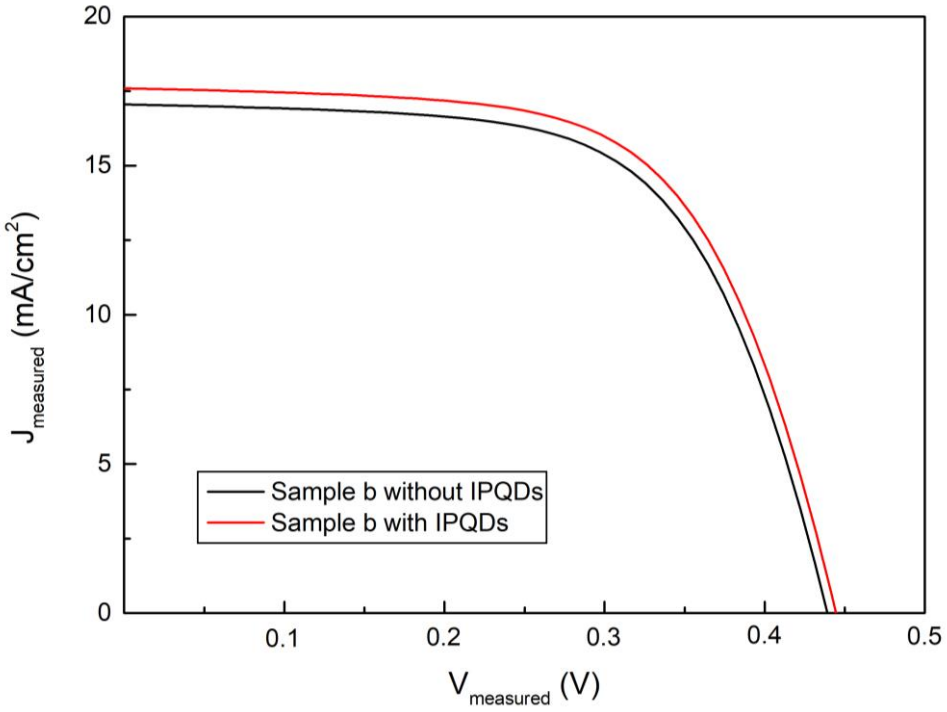

Figure 3.10: Measured I-V curve the LSC device, which comprises the µc-Si:H PV cells with and without the IPQDs coating and the polymeric encapsulation. The represented sample is a set of four individual µc-Si:H PV cells and the demonstrated I-V curves were obtained from the individual cell that better describes the performance of the cells present in the sample. All the measures were performed under a 1000 W/m^2 of incident radiation, in normal with the front surface of each PV cell sample.

The obtained spectral responses for the µc-Si:H PV cells, prior and post deposition of the IPQDs, are displayed in figures 3.11 and 3.12, for both sample A and sample B. An increase in the cells EQE is observable in the 340 to 430 nm range (see Annex K). This is a direct result of light absorption from the luminescent species, which show a strong absorption peak in this wavelength range, more specifically between the 330 and 370 nm.

It is also noticeable an increase in the cells EQE in the 430 to 545 nm range, for sample A, and in the 475 to 600 nm range, for sample B. This is an effect of light trapping resultant from the parylene encapsulation coating.

As it was previously referred, even though both samples are expected to have a similar spectral response, since having been deposited using the same materials and parameters, it is possible that the thin film homogeneity of the silicon cells varies from sample to sample, due to factors inherent to the deposition process itself.

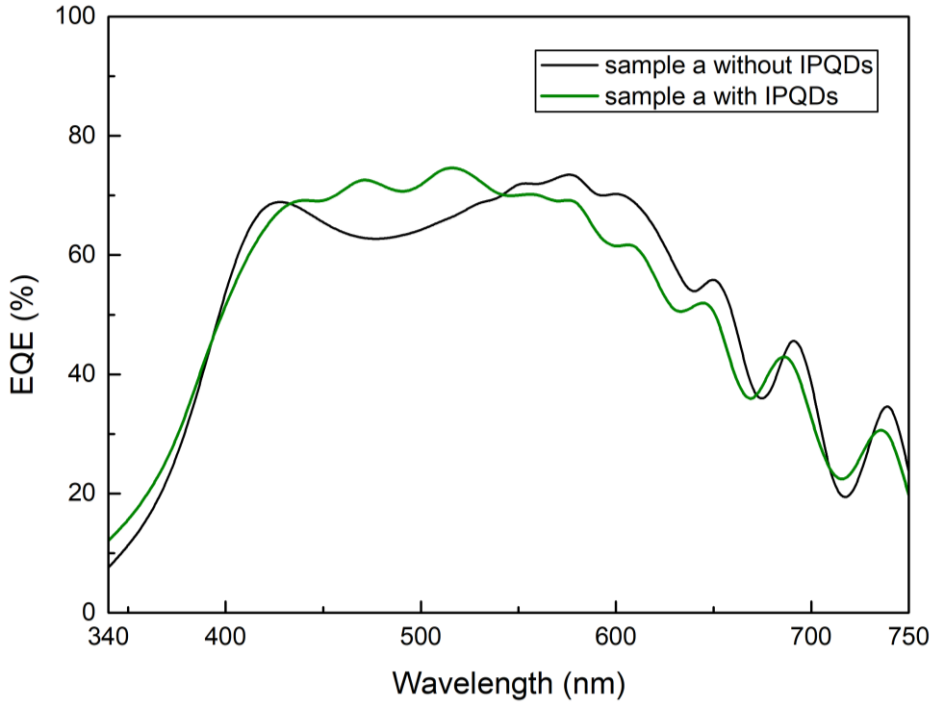

Figure 3.11: Measured spectral response of the µc-Si:H PV cells, for a transmission geometry, prior and post IPQDs deposition and parylene type-C encapsulation. The represented sample is a set of four individual µc-Si:H PV cells and the demonstrated profiles were obtained from the individual cell that better describes the performance of the cells present in the sample.

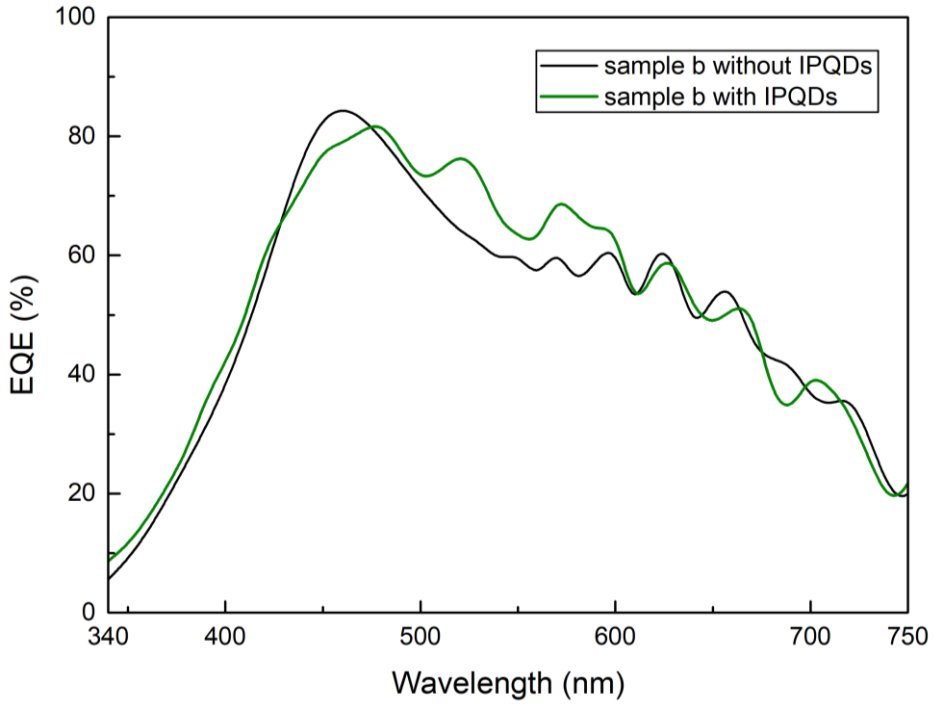

Figure 3.12: Measured spectral response of the µc-Si:H PV cells, for a transmission geometry, prior and post IPQDs deposition and parylene type-C encapsulation. The represented sample is a set of four individual µc-Si:H PV cells and the demonstrated profiles were obtained from the individual cell that better describes the performance of the cells present in the sample.

Table 3.2: Obtained results for the Transmission Geometry, when coupled with an organic PV solar module, for a float glass only sample, a sample composed by a float glass substrate coated with IPQDs and a sample composed by a float glass substrate coated with IPQDs and encapsulated with a parylene type-C thin film.

	Transmission Geometry											
	Uncovered (PV module)			Sample (float glass substrate)			Sample with QDs			Sample with QDs and parylene type-C		
PV Module Parameters	V_{OC} (V)	J_{SC} (mA.cm²)	FF (%)	V_{OC} (V)	J_{SC} (mA.cm²)	FF (%)	V_{OC} (V)	J_{SC} (mA.cm²)	FF (%)	V_{OC} (V)	J_{SC} (mA.cm²)	FF (%)
Average values	0.701	5.90	41.0	0.693	5.12	39.9	0.701	5.38	41.0	0.699	5.47	40.3
Standard Deviation (%)	0.355	1.75	0.5	0.140	3.21	0.3	0.201	4.23	0.2	0.248	7.27	0.2
η_{glass} (%), experimental optical efficiency of the overall system	1.69 ± 0.02			1.41 ± 0.02			1.55 ± 0.02			1.54 ± 0.03		
η_{opt} (%), calculated optical efficiency of the overall system	———			83.6			91.4			91.3		
η_{trans} (%), calculated transmittance of the glass samples	———			81.6			55.4			73.5		

Electric characterization: Luminescence Geometry

From figure 3.13 it is possible to assess the performance of the TLSC device, in the luminescence geometry while coupled to an organic PV solar module, together with the influence of the polymeric coating in the device's measured I-V curve. The data shows that

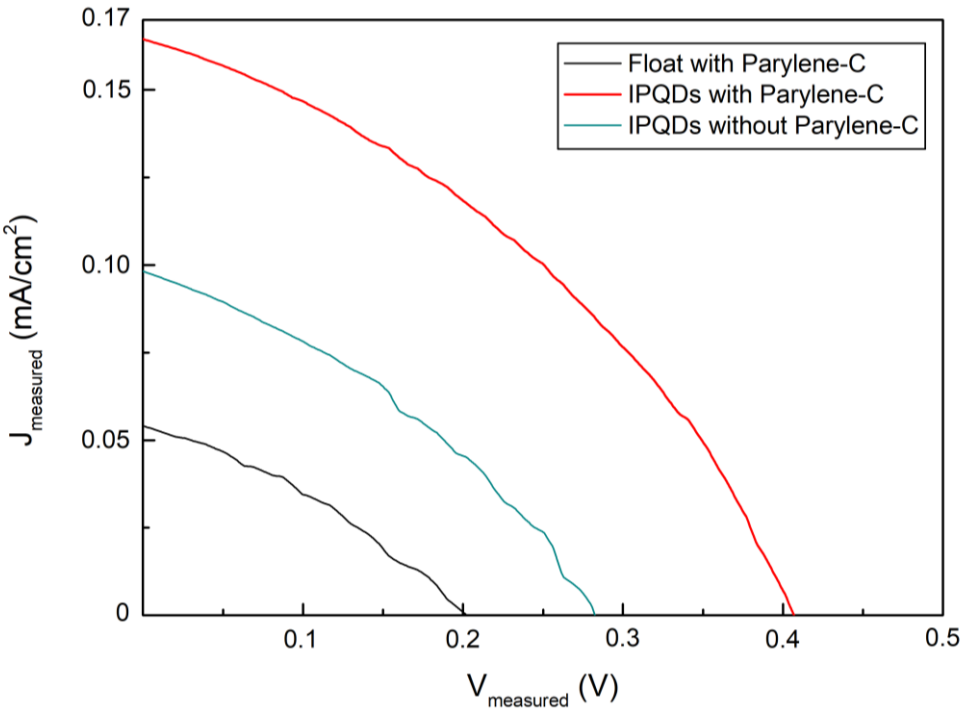

Figure 3.13: Measured I-V curve the TLSC prototype, which comprises both the *InfinityPV* ® tape and the 3D structure, for the samples containing the float glass encapsulated with parylene type-C only, the float glass coated with IPQDs only and the float glass coated with IPQDs and encapsulated with the polymeric coating. All the measures were performed under a 1000 W/m² of incident radiation, in normal with the front surface of each one of the TSC device's assembly.

there is an increase in the current density and voltage values of the assembly when introducing the IPQDs coating to the float substrate, even when this is not encapsulated with the parylene type-C thin film. However, the results suffer an even bigger increase of these values when comparing the TLSC device in which the encapsulation is not present with the TLSC device which comprises both the IPQDs deposition along with the parylene type-C encapsulation. Such rise in both the current density as well as the voltage values, when applying the parylene coating, really comes to show the importance of this encapsulation for the overall TLSC performance.

Table 3.3 displays the calculated values for the optical efficiency, concentration factor and power conversion efficiency of the conceived prototype. These values confirm the enhancement of the device's performance when the IPQDs are used as luminophores, reaching an optical efficiency of 1.73%, for a geometrical factor of 1.313. The value obtained for the TLSC device with the polymeric encapsulation demonstrates and confirms the importance of this coating, reaching an optical efficiency value of 3.72% for the same geometrical factor as the sample containing only the luminophores in thin film.

Table 3.3: Obtained results for the Luminescence Geometry, when coupled with an organic PV solar module, for a sample composed two float glass substrates, a sample composed by two float glass substrates coated with IPQDs and a sample composed by two float glass substrates coated with IPQDs and encapsulated with a parylene type-C thin film. All the measurements were conducted making use of the designed 3D aluminium coated structure.

	Luminescence Geometry		
	Sample (float glass substrate)	Sample with QDs	Sample with QDs and parylene type-C
η_{opt} (%), optical efficiency	_____	1.73	3.72
C_G (%), geometrical concentration factor	_____	2.27	4.89
PCE (%), power conversion efficiency	0.004	0.010	0.026

To the best of our knowledge, this work is ground-breaking since it makes use of inorganic glass materials, as the host-matrix of the developed LSCs and TLSCs, together with an IPQDs thin film derived from a colloidal solution, which is not annealed further enough to achieve a bulk IPQDs thin film. It was possible to obtain a fully transparent LSC with an optical efficiency of 3.72%, in the luminescence configuration, which is competitive with some of the values present in literature. [106]–[108] Furthermore, the developed prototype in the luminescence configuration, after further optimization, might be applied in a small-scale to personal gadgets or in a large-scale in building or automobile integration, for energy saving purposes.

Conc4usion

Inorganic Perovskite $CsPbBr_3$ QDs were synthetized, via hot-injection method, and characterized in terms of their optical properties. The synthetized IPQDs showed a bandgap of 2.42 eV, together with PL emission peaking centred at 500.1 nm and an estimated EQE of 68% in colloidal solution, by the absolute method using an integrating sphere. Afterwards, different glass-comprising substrates were prepared and characterized, prior and posteriorly to the IPQDs deposition, by spin-coating, in order to assess its optical and electrical behaviour, when coupled to a PV device. The two analysed samples were made up of either a float glass sample, which was cleaned with a piranha solution and coated with a mixture of the colloidal IPQDs together with a 10% (w/w) polyethylene and hexane solution, or a glass sample consisting of a 4-set of µc-Si:H PV cells, which were cleaned with isopropanol and coated with the same mixture as the one used for the float glass samples. For security reasons, ultimately to avoid leaking of lead in the handling of the device and to reduce degradation of the luminophores, a polymeric encapsulation of parylene type-C was deposited on top of the IPQDs layer, via CVD.

The obtained transmittance values show an increase, post encapsulation of the samples with the polymeric coating, varying from 84% to 83%, in the visible range, for the float glass samples without and with the parylene type-C coating, respectively, and varying from 52% to 75%, in the visible range, for the float glass coated with IPQDs, without and with the parylene type-C coating, respectively. In terms of the optical properties of the IPQDs deposited thin film with the polymeric coating, a bandgap value of 2.34 eV was obtained, with an PL emission peaking centred at 480.3 nm.

To evaluate the electrical performance of the developed LSCs and TLSCs, the substrates which were constituted only by the float glass matrix, with the IPQDs thin film and parylene type-C encapsulation, were coupled to organic PV modules. The rest of the µc-Si:H comprising substrates were characterized making use of the PV cells electrical contacts, as usual. Two LSC configurations were addressed. To the best of our knowledge, there is not any report in literature where two inorganic glass substrates together with an IPQDs thin film, from a colloidal solution, interlayer are coupled to an PV device, in a window alike configuration, to obtain a TLSC for photovoltaic applications.

For the transmission geometry comprising the inorganic glass substrate coupled to µc-Si:H PV cells, the measured PCE values, prior and posteriorly to the IPQDs thin film deposition and parylene type-C encapsulation, are of 5.08% to 5.25%, respectively, in the case of sample A. For sample B, the PCE values vary from 4.69% to 4.91%, prior and posteriorly to the IPQDs thin film deposition and parylene type-C encapsulation, respectively. This is explained by the contribution of the IPQDs absorption, together with the optical properties of the polymeric thin film, which reduce reflection at the LSC surface, thus increasing transmittance of light into the device. For the same geometry, however coupling the developed float glass LSCs to an organic PV module, the optical efficiency of the LSC system varies from 83.6%, for the PV module alone, to 91.3%, for the overall PV plus LSC system, in which the LSC comprises the IPQDs thin film deposition together with the parylene type-C encapsulation. Regarding the luminescence geometry, an optical efficiency of the overall organic module plus TLSC of 3.72% was obtained, which is in agreement with the values displayed in literature and possible to obtain, from a theoretical standpoint. This configuration also opens a door of opportunity for the implementation of this TLSC, optimized for a large-scale application, in the future building industry for energy saving purposes.

Future perspectives, in a more immediate time frame, include further characterization of the developed technology, with the measure of fluorescence decays, X-ray photoelectron spectroscopy and Raman data acquisition, together with SEM imaging, post IPQDs colloidal solution purification. Regarding electrical characterization, spectral response acquisition is needed for both the samples in transmission geometry and in luminescence geometry, when coupled to an organic PV module. In a medium to short term, optimization of the $CsPbI_3$ IPQDs synthesis is required, as well as studies of doping and capping agents for the reduction of degradation in the synthetized IPQDs and increase of its luminescence QY. Optimization of the thin film deposition from the IPQDs colloidal solution in the µc-Si:H PV samples is also required, together with the study of the optical properties of the used float glass samples as waveguide structures, as well as its durability, its degradation and the presence of impurities and defects in the glass matrix itself. Long term studies require the scale-up of the materials and processes inherent to the devices manufacturing, together with the optimization of the developed prototype and the certification of the final products security, durability and comfortability, for future building integration regarding its photovoltaic applications.

References

[1] A. Pierucci, A. Cannavale, F. Martellotta, and F. Fiorito, "Smart windows for carbon neutral buildings: A life cycle approach," *Energy Build.*, vol. 165, pp. 160–171, 2018.

[2] N. Aste *et al.*, "Design and performance monitoring of a LSC Smart Window," pp. 179–183, 2020.

[3] B. V. Trier, D., Kowalska, M., Rothballer, C., Stiff, G., & Mathiesen, "Guidelines for the Energy System Transition: The National Aspects of the HRE 2050 Scenario and Associated Policy Recommendations - Heat Roadmap Europe 4," Denmark, 2018.

[4] A. Shukla and A. Sharma, *Sustainability through Energy-Efficient Buildings*. Taylor & Francis, 2018.

[5] F. Meinardi, F. Bruni, and S. Brovelli, "Luminescent solar concentrators for building-integrated photovoltaics," *Nature Reviews Materials*, vol. 2. Macmillan Publishers Limited, pp. 1–9, 2017.

[6] P. Moraitis, R. E. I. Schropp, and W. G. J. H. M. van Sark, "Nanoparticles for Luminescent Solar Concentrators - A review," *Opt. Mater. (Amst).*, vol. 84, no. July, pp. 636–645, 2018.

[7] R. Alghamedi, M. Vasiliev, M. Nur-E-Alam, and K. Alameh, "Spectrally-selective all-inorganic scattering luminophores for solar energy-harvesting clear glass windows," *Sci. Rep.*, vol. 4, pp. 1–9, 2014.

[8] C. Olalla, D. Maksimovic, C. Deline, and L. Martinez-Salamero, "Impact of distributed power electronics on the lifetime and reliability of PV systems," *Prog. Photovoltaics Res. Appl.*, vol. 25, no. 10, pp. 821–835, 2017.

[9] J. L. Banal, B. Zhang, D. J. Jones, K. P. Ghiggino, and W. W. H. Wong, "Emissive molecular aggregates and energy migration in luminescent solar concentrators," *Acc. Chem. Res.*, vol. 50, no. 1, pp. 49–57, 2017.

[10] L. Xu, Y. Yao, N. D. Bronstein, L. Li, A. P. Alivisatos, and R. G. Nuzzo, "Enhanced Photon Collection in Luminescent Solar Concentrators with Distributed Bragg Reflectors," *ACS Photonics*, vol. 3, no. 2, pp. 278–285, 2016.

[11] C. Yang and R. R. Lunt, "Limits of Visibly Transparent Luminescent Solar Concentrators," *Advanced Optical Materials*, vol. 5, no. 8. pp. 1–10, 2017.

[12] B. McKenna and R. C. Evans, "Towards Efficient Spectral Converters through Materials Design for Luminescent Solar Devices," *Adv. Mater.*, vol. 29, no. 28, pp. 1–23, 2017.

[13] G. Griffini, "Host Matrix Materials for Luminescent Solar Concentrators: Recent Achievements and Forthcoming Challenges," *Front. Mater.*, vol. 6, no. March, pp. 1–8, 2019.

[14] G. Liu, R. Mazzaro, Y. Wang, H. Zhao, and A. Vomiero, "High efficiency sandwich structure luminescent solar concentrators based on colloidal quantum dots," *Nano Energy*, vol. 60, pp. 119–126, 2019.

[15] J. J. H. Videira, E. Bilotti, and A. J. Chatten, "Cylindrical array luminescent solar concentrators: performance boosts by geometric effects," *Opt. Express*, vol. 24, no. 14,

p. A1188, 2016.

[16] L. R. Bradshaw, K. E. Knowles, S. McDowall, and D. R. Gamelin, "Nanocrystals for luminescent solar concentrators," *Nano Lett.*, vol. 15, no. 2, pp. 1315–1323, 2015.

[17] R. Rondão *et al.*, "High-Performance Near-Infrared Luminescent Solar Concentrators," *ACS Appl. Mater. Interfaces*, vol. 9, no. 14, pp. 12540–12546, 2017.

[18] F. Proise, A.-L. Joudrier, J.-L. Pelouard, and J.-F. Guillemoles, "Loss analysis in luminescent sheet concentrators: from ideal to real system," *EPJ Photovoltaics*, vol. 9, p. 12, 2018.

[19] "Suntuitive Glass." [Online]. Available: https://suntuitiveglass.com/.

[20] S. F. H. Correia, V. De Zea Bermudez, S. J. L. Ribeiro, P. S. André, R. A. S. Ferreira, and L. D. Carlos, "Luminescent solar concentrators: Challenges for lanthanide-based organic-inorganic hybrid materials," *J. Mater. Chem. A*, vol. 2, no. 16, pp. 5580–5596, 2014.

[21] A. R. Frias *et al.*, "Sustainable Liquid Luminescent Solar Concentrators," *Adv. Sustain. Syst.*, vol. 3, no. 3, p. 1800134, 2019.

[22] R. Reisfeld, D. Shamrakov, and C. Jorgensen, "Photostable solar concentrators based on fluorescent glass films," *Sol. Energy Mater. Sol. Cells*, vol. 33, no. 4, pp. 417–427, 1994.

[23] C. Yang and R. R. Lunt, "Limits of Visibly Transparent Luminescent Solar Concentrators," *Adv. Opt. Mater.*, vol. 5, no. 8, pp. 1–10, 2017.

[24] K. Wu, H. Li, and V. I. Klimov, "Tandem luminescent solar concentrators based on engineered quantum dots," *Nat. Photonics*, vol. 12, no. 2, pp. 105–110, 2018.

[25] W. Shockley and H. J. Queisser, "Detailed balance limit of efficiency of p-n junction solar cells," *J. Appl. Phys.*, vol. 32, no. 3, pp. 510–519, 1961.

[26] C. A. Nelson, N. R. Monahan, and X. Y. Zhu, "Exceeding the Shockley-Queisser limit in solar energy conversion," *Energy and Environmental Science*, vol. 6, no. 12. pp. 3508–3519, 2013.

[27] N. Li, Y. S. Lau, Y. Miao, and F. Zhu, "Electroluminescence and photo-response of inorganic halide perovskite bi-functional diodes," *Nanophotonics*, vol. 7, no. 12, pp. 1981–1988, 2018.

[28] J. Pan *et al.*, "Air-Stable Surface-Passivated Perovskite Quantum Dots for Ultra-Robust, Single- and Two-Photon-Induced Amplified Spontaneous Emission," *J. Phys. Chem. Lett.*, vol. 6, no. 24, pp. 5027–5033, 2015.

[29] J. B. Hoffman, G. Zaiats, I. Wappes, and P. V. Kamat, "CsPbBr3 Solar Cells: Controlled Film Growth through Layer-by-Layer Quantum Dot Deposition," *Chem. Mater.*, vol. 29, no. 22, pp. 9767–9774, 2017.

[30] Y. Kim *et al.*, "Efficient Luminescence from Perovskite Quantum Dot Solids," *ACS Appl. Mater. Interfaces*, vol. 7, no. 45, pp. 25007–25013, 2015.

[31] S. Ananthakumar, J. R. Kumar, and S. M. Babu, " Cesium lead halide (CsPbX 3 , X = Cl , Br, I) perovskite quantum dots-synthesis, properties, and applications: a review of their present status ," *J. Photonics Energy*, vol. 6, no. 4, p. 042001, 2016.

[32] L. C. Chen, K. L. Lee, C. Y. Huang, J. C. Lin, and Z. L. Tseng, "Preparation and characteristics of MAPbBr3 perovskite quantum dots on NiOx film and application for high transparent solar cells," *Micromachines*, vol. 9, no. 5, pp. 3–10, 2018.

[33] P. Cottingham and R. L. Brutchey, "On the crystal structure of colloidally prepared CsPbBr3 quantum dots," *Chem. Commun.*, vol. 52, no. 30, pp. 5246–5249, 2016.

[34] Y. Iso and T. Isobe, "Review—Synthesis, Luminescent Properties, and Stabilities of Cesium Lead Halide Perovskite Nanocrystals," *ECS J. Solid State Sci. Technol.*, vol. 7, no. 1, pp. R3040–R3045, 2018.

[35] Z. Li, L. Kong, S. Huang, and L. Li, "Highly Luminescent and Ultrastable CsPbBr3 Perovskite Quantum Dots Incorporated into a Silica/Alumina Monolith," *Angew. Chemie - Int. Ed.*, vol. 56, no. 28, pp. 8134–8138, 2017.

[36] Y. Kim *et al.*, "Efficient Luminescence from Perovskite Quantum Dot Solids (supporting information)," *ACS Appl. Mater. Interfaces*, vol. 7, no. 45, pp. 25007–25013, 2015.

[37] S. N. Raja *et al.*, "Encapsulation of Perovskite Nanocrystals into Macroscale Polymer Matrices: Enhanced Stability and Polarization," *ACS Appl. Mater. Interfaces*, vol. 8, no. 51, pp. 35523–35533, 2016.

[38] W. J. Xu, Z. Y. Du, W. X. Zhang, and X. M. Chen, "Structural phase transitions in perovskite compounds based on diatomic or multiatomic bridges," *CrystEngComm*, vol. 18, no. 41, pp. 7915–7928, 2016.

[39] Y. S. Park, S. Guo, N. S. Makarov, and V. I. Klimov, "Room Temperature Single-Photon Emission from Individual Perovskite Quantum Dots," *ACS Nano*, vol. 9, no. 10, pp. 10386–10393, 2015.

[40] J. Chen *et al.*, "Size and Wavelength Dependent Two-Photon Absorption Cross-Section of CsPbBr Perovskite Quantum Dots Size and Wavelength Dependent Two-Photon Absorption Cross-Section of CsPbBr 3 Perovskite Quantum Dots," 2017.

[41] K. Wu, G. Liang, Q. Shang, Y. Ren, D. Kong, and T. Lian, "Ultrafast interfacial electron and hole transfer from CsPbBr3 perovskite quantum dots," *J. Am. Chem. Soc.*, vol. 137, no. 40, pp. 12792–12795, 2015.

[42] A. Swarnkar *et al.*, "Quantum dot–induced phase stabilization of alpha-CsPbI3 perovskite for high-efficiency photovoltaics," *Science (80-.).*, vol. 354, no. 6308, pp. 92 LP---- 95, 2016.

[43] S. Seth, T. Ahmed, A. De, and A. Samanta, " Tackling the Defects, Stability, and Photoluminescence of CsPbX 3 Perovskite Nanocrystals ," *ACS Energy Lett.*, pp. 1610–1618, 2019.

[44] A. Cannavale, U. Ayr, and F. Martellotta, "Energetic and visual comfort implications of using perovskite-based building-integrated photovoltaic glazings," *Energy Procedia*, vol. 126, pp. 636–643, 2017.

[45] S. Zou *et al.*, "Stabilizing Cesium Lead Halide Perovskite Lattice through Mn(II) Substitution for Air-Stable Light-Emitting Diodes," *J. Am. Chem. Soc.*, vol. 139, no. 33, pp. 11443–11450, 2017.

[46] InfinityPV, "Organic solar cells," *InfinityPV ApS*. InfinityPV, Denmark, p. 1, 2015.

[47] G. U. AGC, "Architectural Coated Glass." AGC Glass Unlimited, p. 40, 2017.

[48] Y. C. Huang and T.-H. Wang, "Automatic calculation of a new China glare index," *Proc. 3rd Ibpsa-engl. Conf.*, vol. 4000, no. 23, p. 22, 2016.

[49] G. C. J. Skarning, C. A. Hviid, and S. Svendsen, "Roadmap for improving roof and façade windows in nearly zero-energy houses in Europe," *Energy Build.*, vol. 116, pp. 602–613, 2016.

[50] S. S. Korsavi, Z. S. Zomorodian, and M. Tahsildoost, "Visual comfort assessment of daylit and sunlit areas: A longitudinal field survey in classrooms in Kashan, Iran," *Energy Build.*, vol. 128, pp. 305–318, 2016.

[51] K. Connelly, Y. Wu, X. Ma, and Y. Lei, "Transmittance and reflectance studies of thermotropic material for a novel building integrated concentrating photovoltaic (BICPV) 'smart window' system," *Energies*, vol. 10, no. 11, 2017.

[52] K. Allen, K. Connelly, P. Rutherford, and Y. Wu, "Smart windows—Dynamic control of building energy performance," *Energy Build.*, vol. 139, pp. 535–546, 2017.

[53] O. M. Olofinnade, A. N. Ede, and J. M. Ndambuki, "Sustainable green environment through utilization of waste soda-lime glass for production of concrete," *J. Mater. Environ. Sci.*, vol. 8, no. 4, pp. 1139–1152, 2017.

[54] J. Singh and R. Singh, "a Review on Recycling of Waste Glass in Construction Industry," *Int. J. Adv. Res. Eng. Appl. Sci.*, vol. 5, no. 7, pp. 37–44, 2016.

[55] H. C. de Sousa Pereira Meneses e Vasconcelos and M. C. Gonçalves, *Overall Aspects of Non-Traditional Glasses: Synthesis, Properties and Applications*. Bentham Science Publishers, 2016.

[56] M. Zhenqiang and D. Liu, *Inorganic Flexible Optoelectronics: Materials and Applications*. John Wiley & Sons, 2019.

[57] B. Lu, Z. Yin, H. Zou, L. Zhi, and J. Feng, "Characterization of Parylene C as protective layer on micro-piezoelectric printheads," *Mater. Sci. Semicond. Process.*, vol. 40, pp. 811–816, 2015.

[58] M. Sun, S. Zhu, C. Zhang, A. Olah, E. Baer, and D. A. Schiraldi, "HDPE/EVOH Multilayered, High Barrier Films for Flexible Organic Photovoltaic Device Packaging," *ACS Appl. Polym. Mater.*, vol. 1, no. 2, pp. 259–266, 2019.

[59] V. Steinmann and L. Moro, "Encapsulation requirements to enable stable organic ultra-thin and stretchable devices," *J. Mater. Res.*, vol. 33, no. 13, pp. 1925–1936, 2018.

[60] R. Mazzaro and A. Vomiero, "The Renaissance of Luminescent Solar Concentrators: The Role of Inorganic Nanomaterials," *Adv. Energy Mater.*, vol. 8, no. 33, pp. 1–19, 2018.

[61] "Soda-lime clear glass refraction index." [Online]. Available: https://refractiveindex.info/?shelf=3d&book=glass&page=soda-lime-clear.

[62] N. A. C. Hirst, "Energy Technology," *The Energy Conundrum*, pp. 119–190, 2018.

[63] B. V. G. Mohan, V. Vasu, A. Robson Benjamin, and M. Kottaisamy, "Luminescent solar concentrators-the solar waveguides," *Curr. Sci.*, vol. 114, no. 8, pp. 1656–1664, 2018.

[64] T. A. Geervliet, I. Gavrila, G. Iasilli, F. Picchioni, and A. Pucci, "Luminescent Solar Concentrators Based on Renewable Polyester Matrices," *Chem. - An Asian J.*, vol. 14, no. 6, pp. 877–883, 2019.

[65] P. Della Sala *et al.*, "First demonstration of the use of very large Stokes shift cycloparaphenylenes as promising organic luminophores for transparent luminescent solar concentrators," *Chem. Commun.*, vol. 55, no. 21, pp. 3160–3163, 2019.

[66] L. R. Bradshaw, K. E. Knowles, S. McDowall, and D. R. Gamelin, "Nanocrystals for luminescent solar concentrators," *Nano Lett.*, vol. 15, no. 2, pp. 1315–1323, 2015.

[67] Z. Krumer, W. G. J. H. M. van Sark, R. E. I. Schropp, and C. de Mello Donegá, "Compensation of self-absorption losses in luminescent solar concentrators by increasing luminophore concentration," *Sol. Energy Mater. Sol. Cells*, vol. 167, no. July 2016, pp. 133–139, 2017.

[68] M. Debije, "Luminescent solar concentrators: Semiconductor solution," *Nat. Photonics*, vol. 11, no. 3, pp. 143–144, 2017.

[69] C. J. Traverse, R. Pandey, M. C. Barr, and R. R. Lunt, "Emergence of highly transparent photovoltaics for distributed applications," *Nat. Energy*, vol. 2, no. 11, pp. 849–860, 2017.

[70] H. Huang, K. Cai, Y. Sie, K. Li, J. Yeh, and C. Yuan, "Eco-Friendly, High-Loading Luminescent Solar Concentrators with Concurrently Enhanced Optical Density and Quantum Yields While Without Sacrificing Edge-Emission Efficiency," *Sol. RRL*, vol. 3, no. 5, p. 1800347, 2019.

[71] S. F. H. Correia, P. P. Lima, P. S. André, M. R. S. Ferreira, and L. A. D. Carlos, "High-efficiency luminescent solar concentrators for flexible waveguiding photovoltaics," *Sol. Energy Mater. Sol. Cells*, vol. 138, pp. 51–57, 2015.

[72] Y. Dong, T. Qiao, D. Kim, D. Parobek, D. Rossi, and D. H. Son, "Precise Control of Quantum Confinement in Cesium Lead Halide Perovskite Quantum Dots via Thermodynamic Equilibrium," *Nano Lett.*, vol. 18, no. 6, pp. 3716–3722, 2018.

[73] J. Chen, D. Liu, M. J. Al-Marri, L. Nuuttila, H. Lehtivuori, and K. Zheng, "Photo-stability of CsPbBr3 perovskite quantum dots for optoelectronic application," *Sci. China Mater.*, vol. 59, no. 9, pp. 719–727, 2016.

[74] X. Li *et al.*, "CsPbX3 Quantum Dots for Lighting and Displays: Roomerature Synthesis, Photoluminescence Superiorities, Underlying Origins and White Light-Emitting Diodes," *Adv. Funct. Mater.*, vol. 26, no. 15, pp. 2435–2445, 2016.

[75] A. Swarnkar, R. Chulliyil, V. K. Ravi, M. Irfanullah, A. Chowdhury, and A. Nag, "Colloidal CsPbBr3 Perovskite Nanocrystals: Luminescence beyond Traditional Quantum Dots," *Angew. Chemie - Int. Ed.*, vol. 54, no. 51, pp. 15424–15428, 2015.

[76] C. Sun *et al.*, "Efficient and Stable White LEDs with Silica-Coated Inorganic Perovskite Quantum Dots," *Adv. Mater.*, vol. 28, no. 45, pp. 10088–10094, 2016.

[77] Y. Wang, X. Li, J. Song, L. Xiao, H. Zeng, and H. Sun, "All-Inorganic Colloidal Perovskite Quantum Dots: A New Class of Lasing Materials with Favorable Characteristics," *Adv. Mater.*, vol. 27, no. 44, pp. 7101–7108, 2015.

[78] T. Xuan *et al.*, "Monodisperse and brightly luminescent CsPbBr3/Cs4PbBr6

perovskite composite nanocrystals," *Nanoscale*, vol. 10, no. 21, pp. 9840–9844, 2018.

[79] T. P. Nguyen *et al.*, "Facile synthesis of CsPbBr 3 /PbSe composite clusters," *Sci. Technol. Adv. Mater.*, vol. 19, no. 1, pp. 10–17, 2018.

[80] X. He, Y. Qiu, and S. Yang, "Fully-Inorganic Trihalide Perovskite Nanocrystals: A New Research Frontier of Optoelectronic Materials," *Adv. Mater.*, vol. 29, no. 32, pp. 1–27, 2017.

[81] G. Longo, M. G. La-Placa, M. Sessolo, and H. J. Bolink, "High Photoluminescence Quantum Yields in Organic Semiconductor–Perovskite Composite Thin Films," *ChemSusChem*, vol. 10, no. 19, pp. 3788–3793, 2017.

[82] I. Papakonstantinou and C. Tummeltshammer, "Fundamental limits of concentration in luminescent solar concentrators revised: the effect of reabsorption and nonunity quantum yield," *Optica*, vol. 2, no. 10, p. 841, 2015.

[83] R. Sumner *et al.*, "Analysis of Optical Losses in High-Efficiency CuInS2-Based Nanocrystal Luminescent Solar Concentrators: Balancing Absorption versus Scattering," *J. Phys. Chem. C*, vol. 121, no. 6, pp. 3252–3260, 2017.

[84] E. Fanizza *et al.*, "Post-synthesis phase and shape evolution of CsPbBr 3 colloidal nanocrystals: The role of ligands," *Nano Res.*, vol. 12, no. 1, 2019.

[85] X. Fu *et al.*, "Self-assembly and photoactivation of blue luminescent CsPbBr3 mesocrystals synthesized at ambient temperature," *J. Mater. Chem. C*, vol. 6, no. 7, pp. 1701–1708, 2018.

[86] Y. Bekenstein, B. A. Koscher, S. W. Eaton, P. Yang, and A. P. Alivisatos, "Highly Luminescent Colloidal Nanoplates of Perovskite Cesium Lead Halide and Their Oriented Assemblies," *J. Am. Chem. Soc.*, vol. 137, no. 51, pp. 16008–16011, 2015.

[87] V. K. Ravi, A. Swarnkar, R. Chakraborty, and A. Nag, "Excellent green but less impressive blue luminescence from CsPbBr3 perovskite nanocubes and nanoplatelets," *Nanotechnology*, vol. 27, no. 32, 2016.

[88] Z. Liu *et al.*, "Ligand Mediated Transformation of Cesium Lead Bromide Perovskite Nanocrystals to Lead Depleted Cs4PbBr6 Nanocrystals," *J. Am. Chem. Soc.*, vol. 139, no. 15, pp. 5309–5312, 2017.

[89] H. Zhang, Q. Liao, Y. Wu, J. Chen, Q. Gao, and H. Fu, "Pure zero-dimensional Cs4PbBr6 single crystal rhombohedral microdisks with high luminescence and stability," *Phys. Chem. Chem. Phys.*, vol. 19, no. 43, pp. 29092–29098, 2017.

[90] J. Cho and S. Banerjee, "Ligand-Directed Stabilization of Ternary Phases: Synthetic Control of Structural Dimensionality in Solution-Grown Cesium Lead Bromide Nanocrystals," *Chem. Mater.*, vol. 30, no. 17, pp. 6144–6155, 2018.

[91] X. Li *et al.*, "Solution-Processed Perovskite Microdisk for Coherent Light Emission," *Adv. Opt. Mater.*, vol. 1900678, pp. 1–9, 2019.

[92] Y. Ding *et al.*, "Tin-assisted growth of all-inorganic perovskite nanoplatelets with controllable morphologies and complementary emissions," *CrystEngComm*, vol. 21, no. 14, pp. 2388–2397, 2019.

[93] X. Dong *et al.*, "Trivalent ion mediated abnormal growth of all-inorganic perovskite nanocrystals and their divergent emission properties," *Nanoscale*, vol. 11, no. 16, pp.

7903–7912, 2019.

[94] Y. Wu *et al.*, "In Situ Passivation of PbBr 64- Octahedra toward Blue Luminescent CsPbBr 3 Nanoplatelets with Near 100% Absolute Quantum Yield," *ACS Energy Lett.*, vol. 3, no. 9, pp. 2030–2037, 2018.

[95] V. I. Klimov, T. A. Baker, J. Lim, K. A. Velizhanin, and H. McDaniel, "Quality Factor of Luminescent Solar Concentrators and Practical Concentration Limits Attainable with Semiconductor Quantum Dots," *ACS Photonics*, vol. 3, no. 6, pp. 1138–1148, 2016.

[96] L. J. Brennan, F. Purcell-Milton, B. McKenna, T. M. Watson, Y. K. Gun'ko, and R. C. Evans, "Large area quantum dot luminescent solar concentrators for use with dye-sensitised solar cells," *J. Mater. Chem. A*, vol. 6, no. 6, pp. 2671–2680, 2018.

[97] Y. Zhou, H. Zhao, D. Ma, and F. Rosei, "Harnessing the properties of colloidal quantum dots in luminescent solar concentrators," *Chem. Soc. Rev.*, vol. 47, no. 15, pp. 5866–5890, 2018.

[98] H. Zhao, Y. Zhou, D. Benetti, D. Ma, and F. Rosei, "Perovskite quantum dots integrated in large-area luminescent solar concentrators," *Nano Energy*, vol. 37, pp. 214–223, 2017.

[99] H. Zhao and F. Rosei, "Colloidal Quantum Dots for Solar Technologies," *Chem*, vol. 3, no. 2, pp. 229–258, 2017.

[100] Specialty Coating Systems, "SCS Parylene Properties," *Accessed From Http://Scscoatings.Com/Corporate/Library.Aspx*. Specialty Coating Systems, p. 12, 2016.

[101] M. Sygletou, M. E. Kyriazi, A. G. Kanaras, and E. Stratakis, "Anion exchange in inorganic perovskite nanocrystal polymer composites," *Chem. Sci.*, vol. 9, no. 42, pp. 8121–8126, 2018.

[102] T. J. Jacobsson, M. Pazoki, A. Hagfeldt, and T. Edvinsson, "Goldschmidt Rules and Strontium Replacement in Lead Halogen Perovskite Solar Cells: Theory and Preliminary Experiments on CH3NH3SrI3," *J. Phys. Chem. C*, vol. 119, no. 46, pp. 25673–25683, 2015.

[103] D. Chen, S. Zhou, G. Fang, X. Chen, and J. Zhong, "Fast Room-Temperature Cation Exchange Synthesis of Mn-Doped CsPbCl 3 Nanocrystals Driven by Dynamic Halogen Exchange," *ACS Appl. Mater. Interfaces*, vol. 10, no. 46, pp. 39872–39878, 2018.

[104] R. R. Tamming *et al.*, "Ultrafast Spectrally Resolved Photoinduced Complex Refractive Index Changes in CsPbBr 3 Perovskites," *ACS Photonics*, vol. 6, no. 2, pp. 345–350, 2019.

[105] M. J. Jurow *et al.*, "Tunable Anisotropic Photon Emission from Self-Organized CsPbBr 3 Perovskite Nanocrystals," *Nano Lett.*, vol. 17, no. 7, pp. 4534–4540, 2017.

[106] S. Sadeghi *et al.*, "Stokes-Shift-Engineered Indium Phosphide Quantum Dots for Efficient Luminescent Solar Concentrators," *ACS Appl. Mater. Interfaces*, vol. 10, no. 15, pp. 12975–12982, 2018.

[107] C. Yang *et al.*, "Impact of Stokes Shift on the Performance of Near-Infrared Harvesting Transparent Luminescent Solar Concentrators," *Sci. Rep.*, vol. 8, no. 1, pp. 1–10, 2018.

[108] F. Meinardi *et al.*, "Highly efficient luminescent solar concentrators based on earth-Abundant indirect-bandgap silicon quantum dots," *Nat. Photonics*, vol. 11, no. 3, pp. 177–185, 2017.

Annexes

Annex A

Table A.1: Used deposition parameters for the spin-coat deposition of the synthetized IPQDs in inorganic float glass substrates.

Glass sample (nr. of depositions; concentration IPQDs)	IPQDs to 10% (weight) polyethylene-hexane solution ratio	Spin-coater parameters	Thermal anneal
(1 deposition; pellet re-dispersed in 2.5 mL of hexane)	1:2, followed by an thermal anneal	Time: 20 s Velocity: 1500 rpm Acceleration: 500 rpm/s	50 °C during 5 min
(2 depositions; pellet re-dispersed in 2.5 mL of hexane)	A first 1:2 deposition, followed by an thermal anneal and a second 1:2 deposition, followed again by a thermal anneal		

Annex B

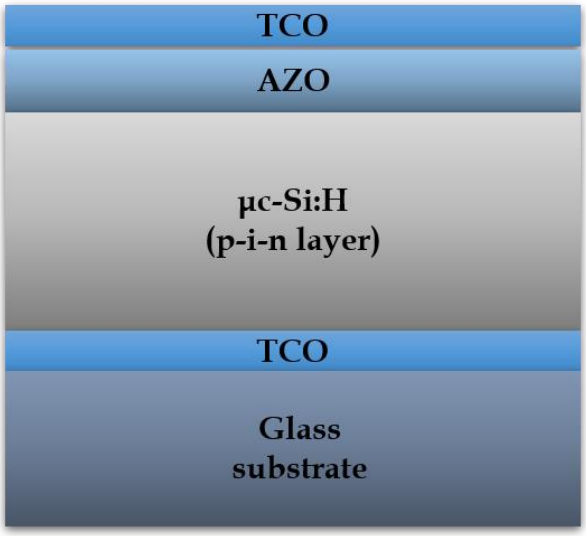

Figure B.1: Schematic representing the layers which constitute the individual µc-Si:H PV cells present in both sample A and B.

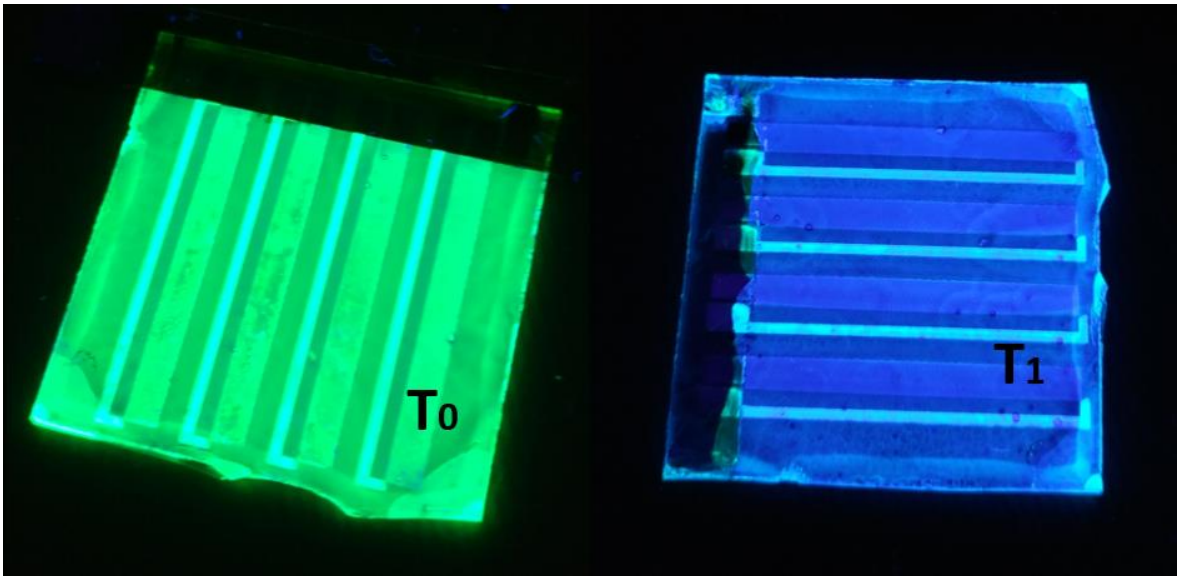

Figure B.2: Sample A, which is a 4-set sample of individual µc-Si:H PV cells after the IPQDs deposition (T_0) and after the parylene coating addition (T_1 equal to 4 days).

Table B.1: Used deposition parameters for the spin-coat deposition of the synthetized IPQDs on top of the IZO layer of the µc-Si:H PV samples A and B.

Glass sample with deposited µc-Si:H PV cells (nr. of depositions; concentration IPQDs)	IPQDs to 10% (weight) polyethylene-hexane solution ratio	Spin-coater parameters	Thermal anneal
(1 deposition; pellet re-dispersed in 5 mL of hexane)	1:2, followed by an thermal anneal	Time: 30 s Velocity: 1500 rpm Acceleration: 500 rpm/s	50 °C during 5 min

Annex C

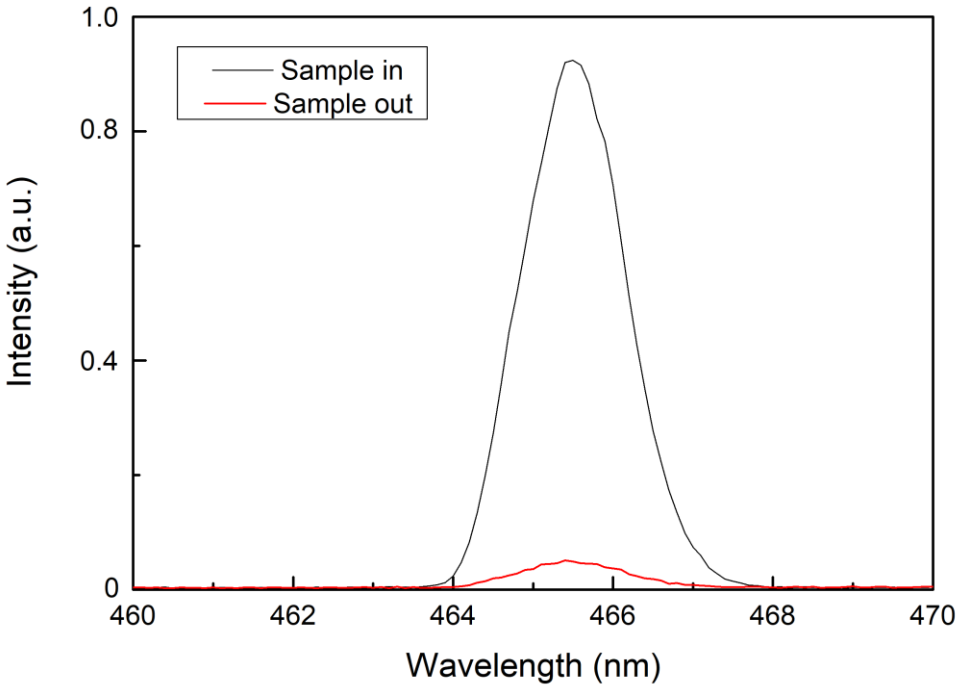

Figure C.1: Emission spectra of the highest concentration colloidal sample (black line) and the background spectrum (red line).

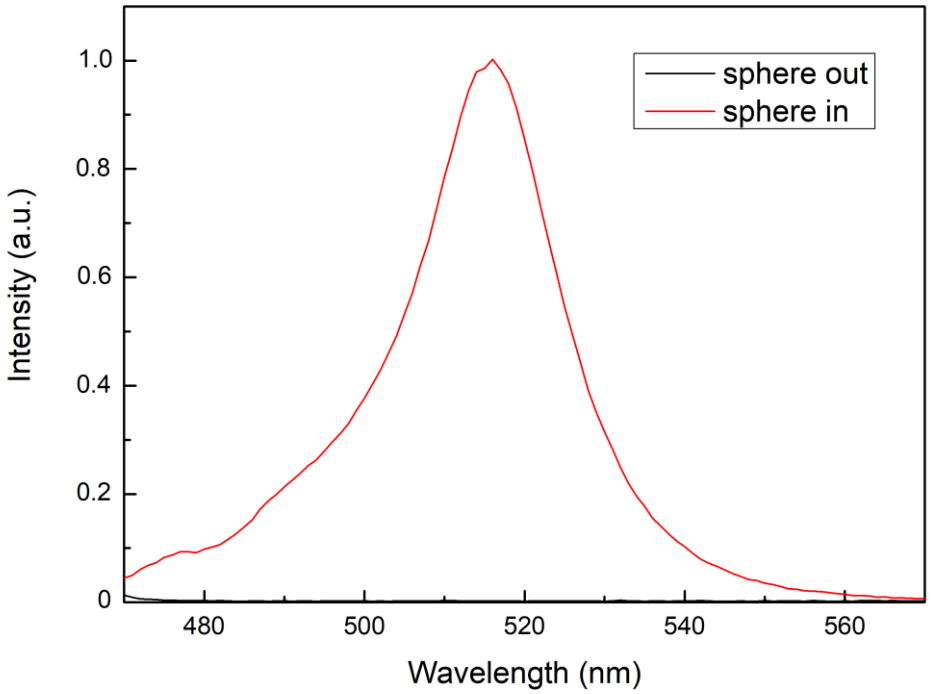

Figure C.2: Emission spectra of the highest concentration colloidal sample in the presence of an integrating sphere (red line) and of the background spectrum, without integrating sphere that is (black line).

Annex D

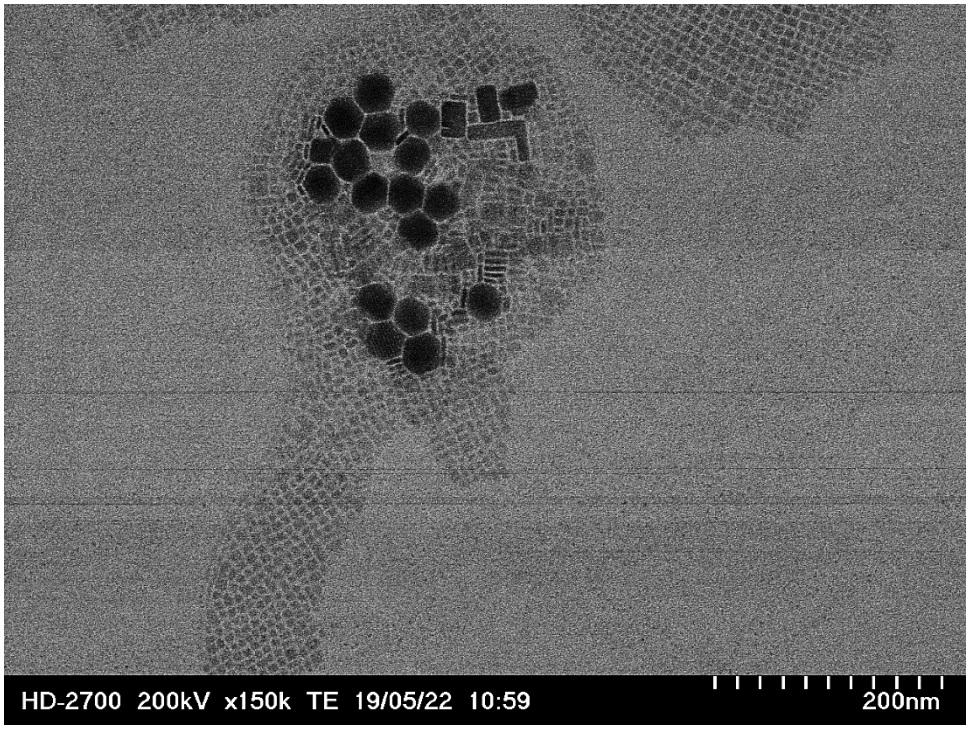

Figure D.1: STEM image obtained from the highest concentration solution (pellet re-dispersed in 2.5 mL of hexane).

Annex E

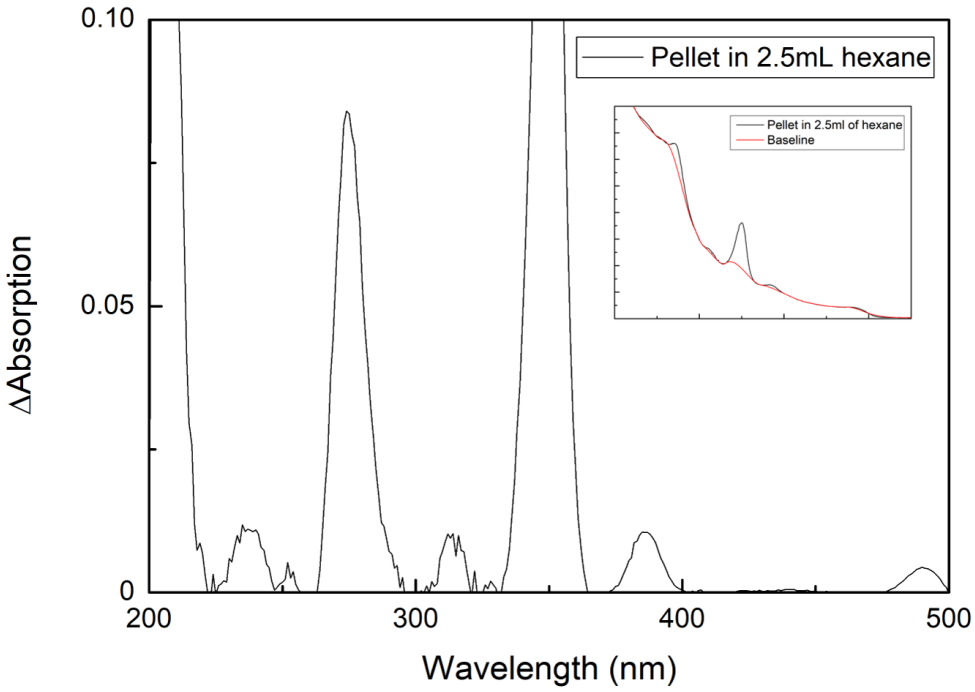

Figure E.1: Visible absorption peaking resultant from the baseline subtraction of the original absorption data, for the highest concentration colloidal solution (pellet re-dispersed in 2.5 mL of hexane).

Annex F

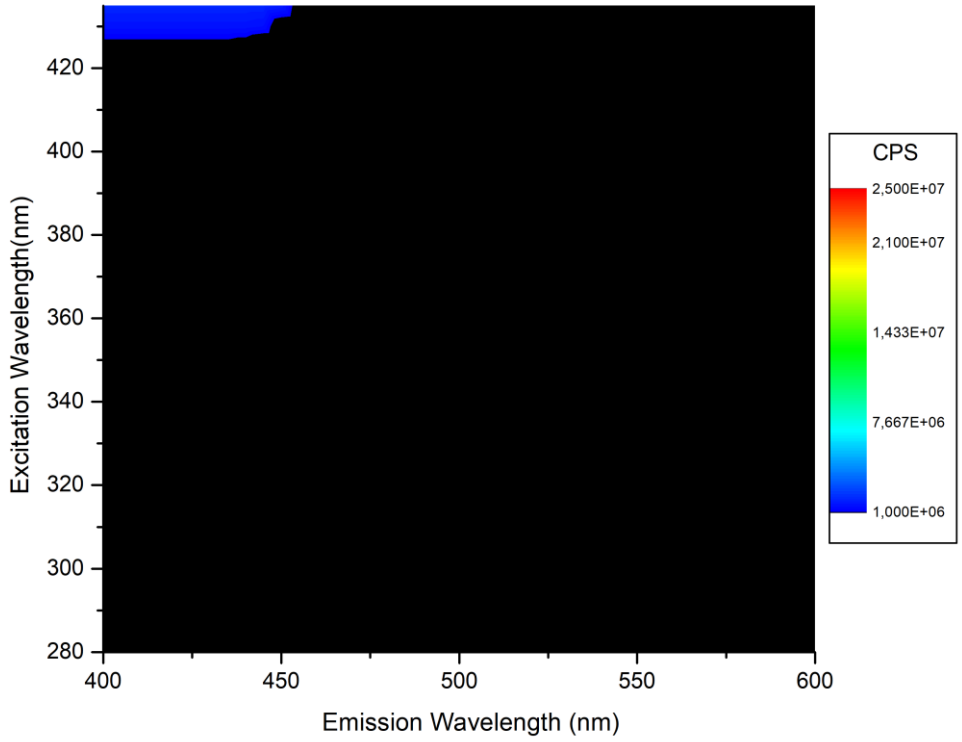

Figure F.1: 3D PL contour plot obtained for the blank float glass sample, without IPQDs deposition or parylene type-C encapsulation that is.

Annex G

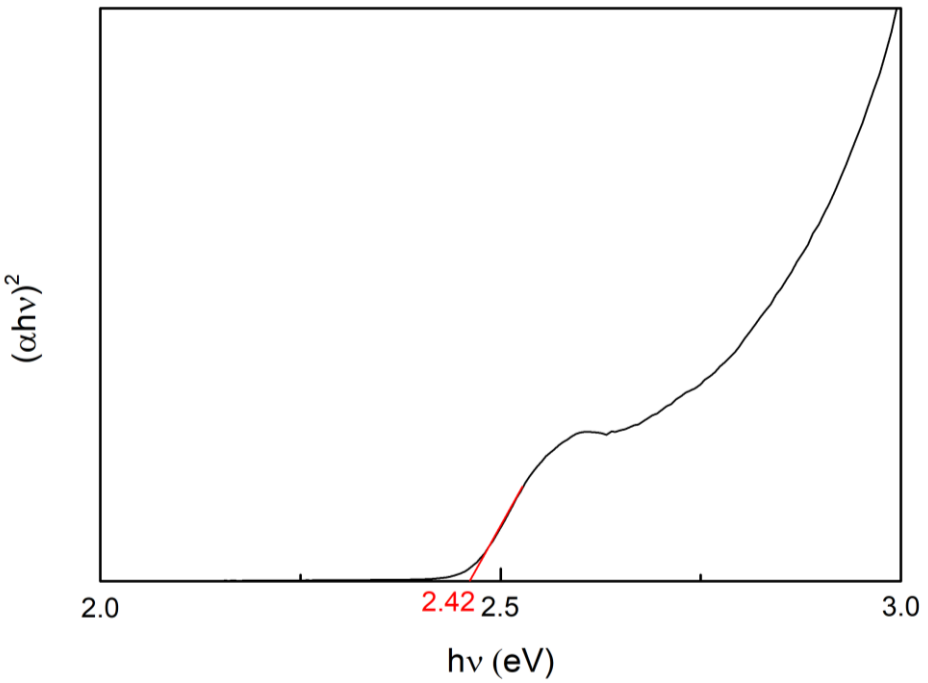

Figure G.1: Tauc plot of the highest concentration IPQDs colloidal solution (pellet re-dispersed in 2.5 mL of hexane).

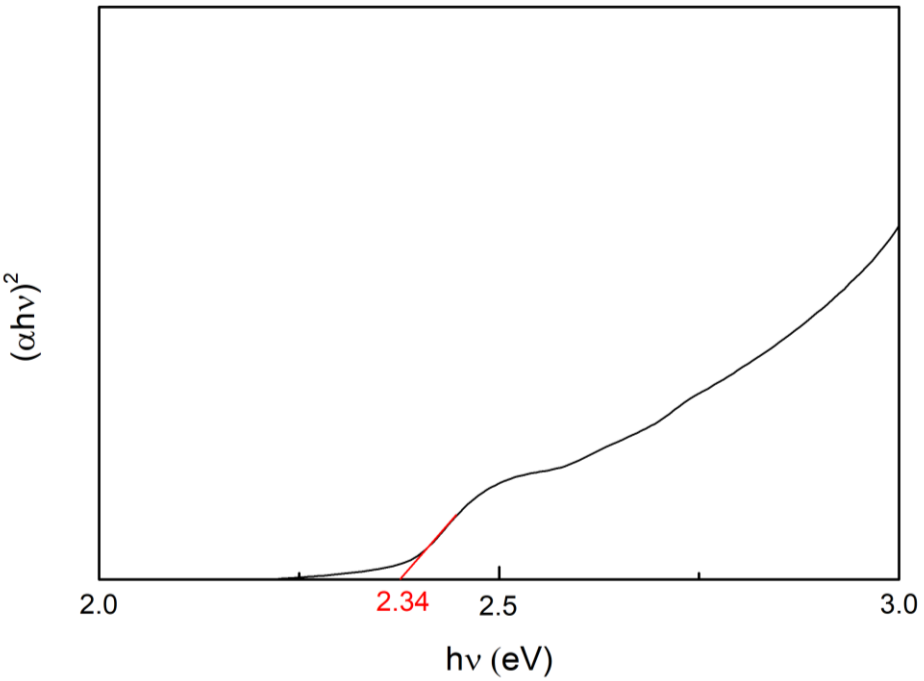

Figure G.2: Tauc plot of the highest concentration IPQDs thin film deposition, in float glass substrate, without the parylene type-C encapsulation.

Annex H

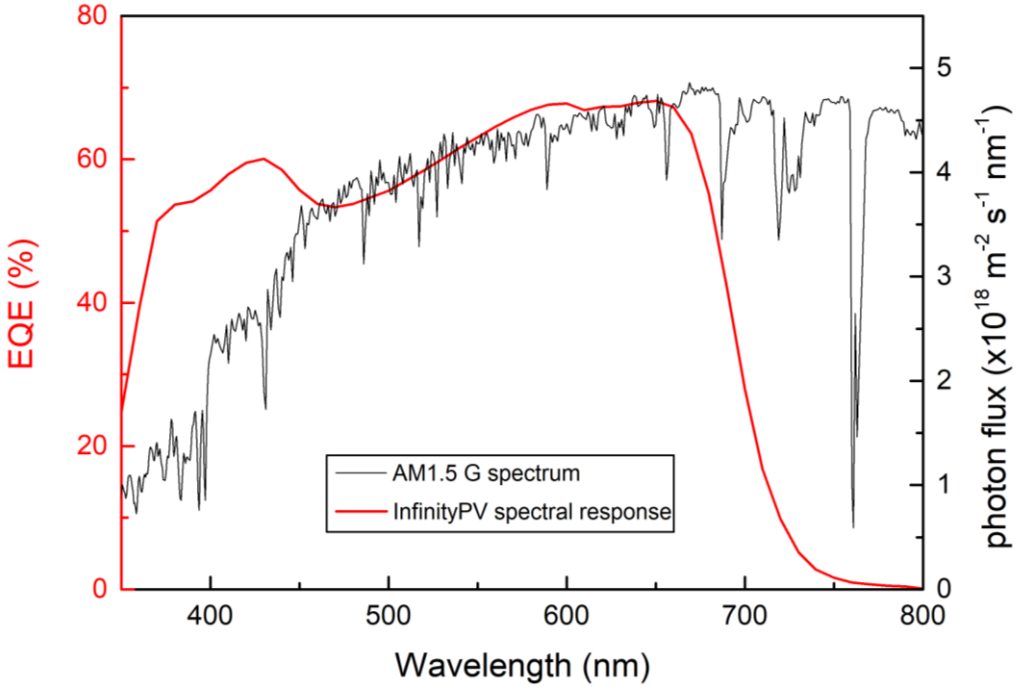

Figure H.1: Measured spectral response of the used InfinityPV ® organic module in comparison to the AM1.5G solar spectrum.

Annex I

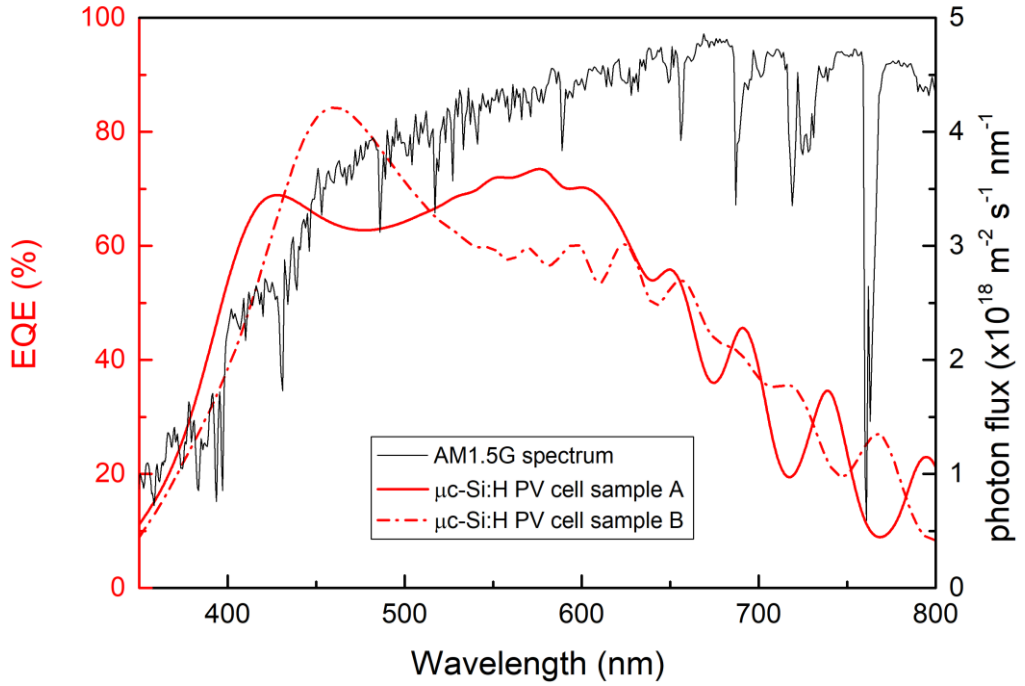

Figure I.1: Measured spectral responses for the µc-Si:H PV cells comprising samples, A and B, in comparison to the AM1.5G solar spectrum.

Annex J

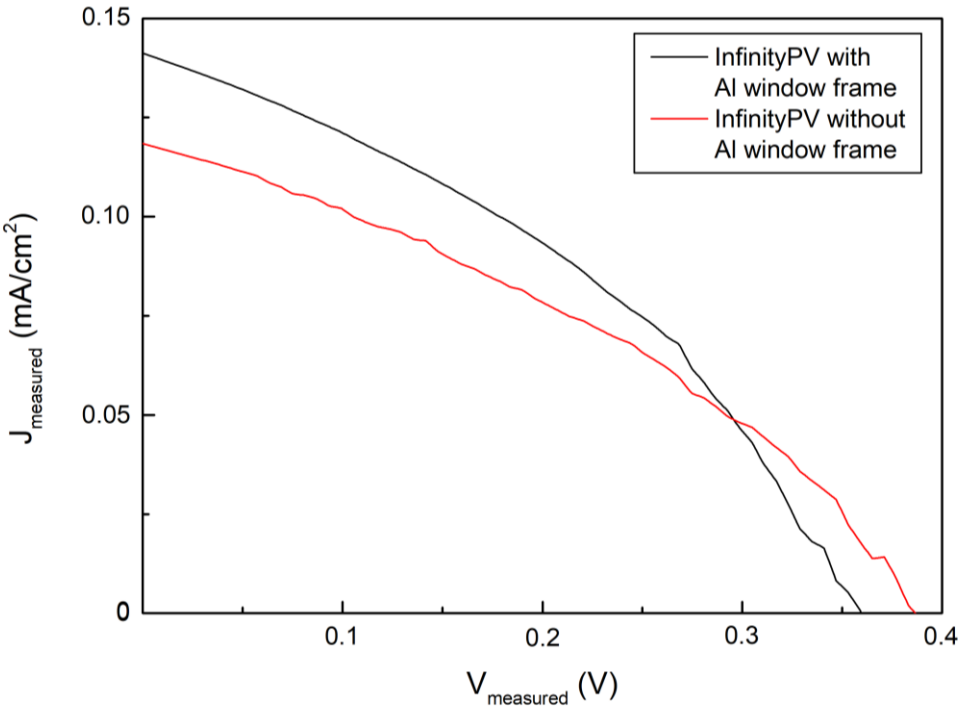

Figure J.1: Measured I-V curves for the InfinityPV ® organic module, placed in parallel with the incident radiation, with and without the presence of the aluminium covered framework-like structure.

Annex K

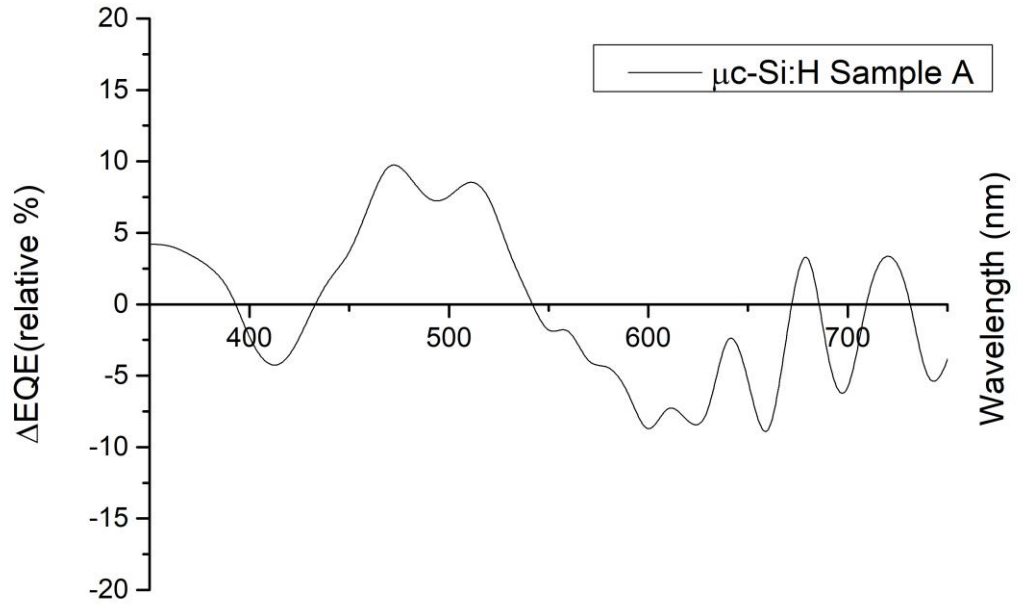

Figure K.1: Spectral response variation of the μc-Si:H PV cells comprising sample A, obtained from the subtraction of the measured spectral response with and without the IPQDs deposition and parylene type-C encapsulation.

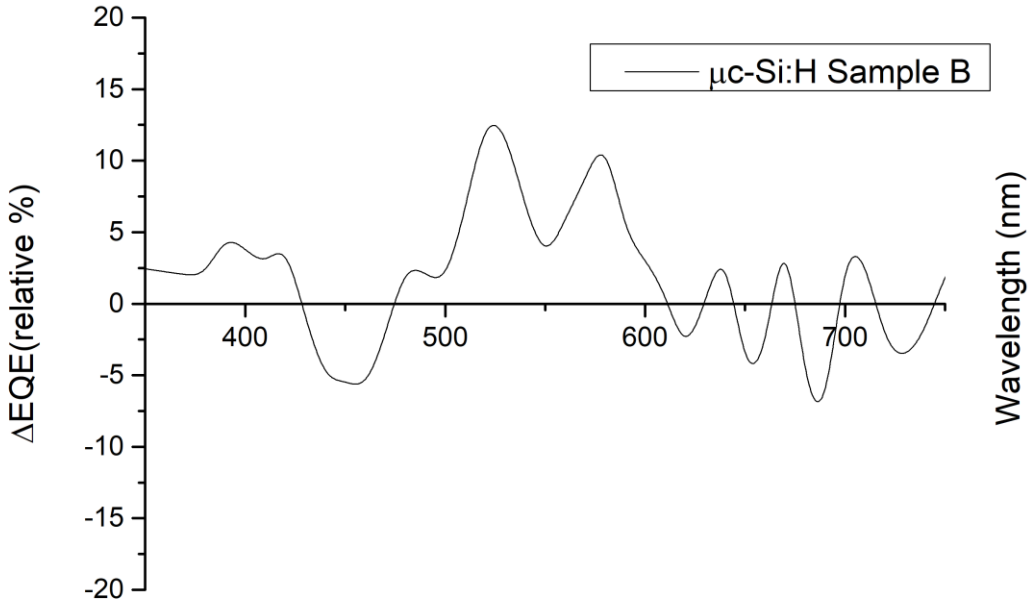

Figure K.2: Spectral response variation of the μc-Si:H PV cells comprising sample B, obtained from the subtraction of the measured spectral response with and without the IPQDs deposition and parylene type-C encapsulation.